Short Article

Molecular Cell

Plasticity of the Cullin-RING Ligase Repertoire Shapes Sensitivity to Ligand-Induced Protein Degradation

Graphical Abstract

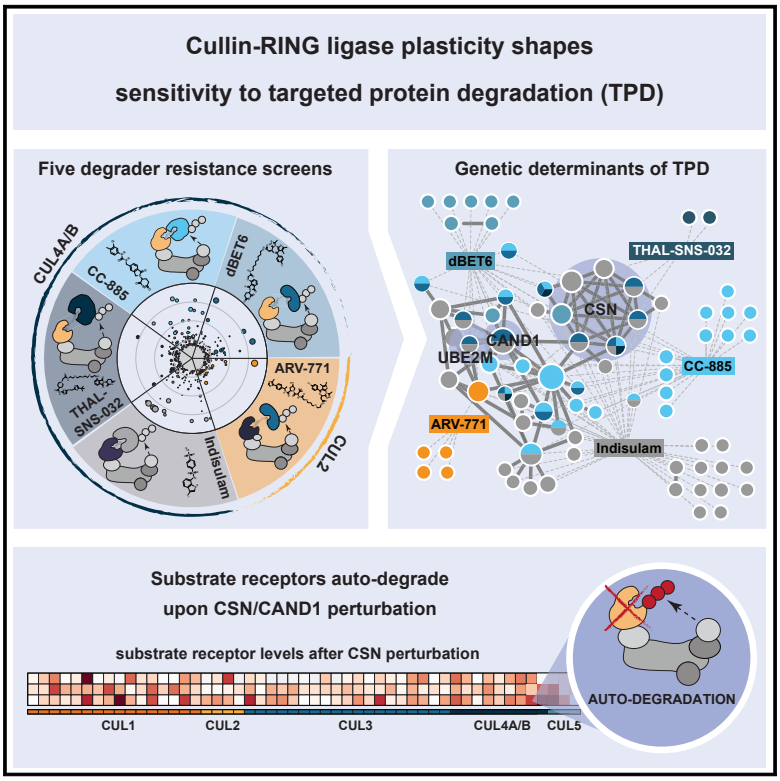

Highlights

- Unbiased survey reveals global and specific effectors for target degradation
- CRL dependency on CAND1/CSN is ligase and context specific
- Perturbing CAND1/CSN abrogates CRL plasticity and prompts ligase auto-degradation
- CSN inactivation blocks substrate-driven CRL assembly

Authors

Cristina Mayor-Ruiz, Martin G. Jaeger, Sophie Bauer, ..., André C. Mueller, Jörg Menche, Georg E. Winter

Correspondence

cmayor-ruiz@cemm.oeaw.ac.at (C.M.-R.), gwinter@cemm.oeaw.ac.at (G.E.W.)

In Brief

Mayor-Ruiz et al. combine functional genomics and quantitative proteomics to identify cellular modulators of ligand-induced targeted protein degradation. Several regulators, such as CAND1 and the COP9 signalosome, maintain context-specific ligase plasticity to enable substrate-driven ligase assembly and protect substrate receptors from auto-degradation.

Mayor-Ruiz et al., 2019, Molecular Cell *75*, 849–858
August 22, 2019
https://doi.org/10.1016/j.molcel.2019.07.013

CellPress

Molecular Cell
Short Article

Plasticity of the Cullin-RING Ligase Repertoire Shapes Sensitivity to Ligand-Induced Protein Degradation

Cristina Mayor-Ruiz,[1,2,*] Martin G. Jaeger,[1,2] Sophie Bauer,[1] Matthias Brand,[1] Celine Sin,[1] Alexander Hanzl,[1] André C. Mueller,[1] Jörg Menche,[1] and Georg E. Winter[1,3,*]
[1]CeMM Research Center for Molecular Medicine of the Austrian Academy of Sciences, Lazarettgasse 14, AKH BT 25.3, 1090 Vienna, Austria
[2]These authors contributed equally
[3]Lead Contact
*Correspondence: cmayor-ruiz@cemm.oeaw.ac.at (C.M.-R.), gwinter@cemm.oeaw.ac.at (G.E.W.)
https://doi.org/10.1016/j.molcel.2019.07.013

SUMMARY

Inducing protein degradation via small molecules is a transformative therapeutic paradigm. Although structural requirements of target degradation are emerging, mechanisms determining the cellular response to small-molecule degraders remain poorly understood. To systematically delineate effectors required for targeted protein degradation, we applied genome-scale CRISPR/Cas9 screens for five drugs that hijack different substrate receptors (SRs) of cullin RING ligases (CRLs) to induce target proteolysis. We found that sensitivity to small-molecule degraders is dictated by shared and drug-specific modulator networks, including the COP9 signalosome and the SR exchange factor CAND1. Genetic or pharmacologic perturbation of these effectors impairs CRL plasticity and arrests a wide array of ligases in a constitutively active state. Resulting defects in CRL decommissioning prompt widespread CRL auto-degradation that confers resistance to multiple degraders. Collectively, our study informs on regulation and architecture of CRLs amenable for targeted protein degradation and outlines biomarkers and putative resistance mechanisms for upcoming clinical investigation.

INTRODUCTION

Targeted protein degradation (TPD) represents a novel paradigm in drug development. It is based on small molecules, often called degraders, which redirect the activity of E3 ubiquitin ligases to induce selective protein degradation. Mechanistically, degraders function by inducing molecular proximity between an E3 ligase and a neosubstrate protein, prompting ubiquitin transfer and subsequent proteasomal degradation of the target. Depending on their design, degraders are either classified as non-chimeric molecular glues, or heterobifunctional PROTACs (proteolysis-targeting chimeras), which connect a targeting warhead with an E3 ligase binder via a flexible linker (Sakamoto et al., 2001). This heterobifunctional design enables rational degrader development for a wide array of targets (Bondeson et al., 2015; Lu et al., 2015; Winter et al., 2015; Zengerle et al., 2015). Clinical proof of concept for TPD is provided by the anti-myeloma drug lenalidomide and related immunomodulatory drugs (IMiDs). IMiDs redirect the E3 ligase CRBN to degrade a range of proteins, including transcription factors, via a glue-like mechanism (Ito et al., 2010; Krönke et al., 2014; Lu et al., 2014; Sievers et al., 2018b). Both types of degraders promise to overcome limitations of conventional drug development. Pharmacologically, degraders differ from traditional antagonists as they act catalytically (Bondeson et al., 2015). Although structural determinants of target recruitment and degrader efficacy are emerging (Gadd et al., 2017; Matyskiela et al., 2016; Nowak et al., 2018; Petzold et al., 2016; Roy et al., 2019), cellular effectors required to support the unique pharmacology of TPD remain elusive.

The ubiquitin-proteasome pathway orchestrates protein degradation with exquisite specificity. Target ubiquitination requires an E1 ubiquitin-activating enzyme, an E2 ubiquitin-conjugating enzyme, and an E3 ubiquitin ligase (Hershko et al., 2000; Komander and Rape, 2012). Currently, TPD only utilizes a small subset of the 600 specificity-conferring E3s, most of which are cullin-RING ligases (CRLs). CRLs are modular protein assemblies, where a cullin scaffold mediates contacts between an E2 enzyme (via a RING protein) and the target (via a substrate receptor; Fischer et al., 2011; Zheng et al., 2002b). TPD chemically modulates the target space of CRL substrate receptors (SRs) to trigger degradation of novel targets. Based on the integrated cullin, CRLs are divided into seven classes. Each class is further diversified by modular assembly with their respective SRs, which ultimately direct CRL ligase activity. Current understanding of CRL biology is mostly derived from a few model complexes. CUL1-associated ligases utilizing F-box SRs have served as prototypical specimens and are referred to as SCF (Skp1:Cul1:F-box) ligases. Studies on SCF ligases revealed a remarkably dynamic regulation that allows rapid adaptation to cellular needs. SCF activity requires the reversible attachment of the ubiquitin-like protein NEDD8 to the cullin scaffold (Deshaies et al., 2010; Pierce et al., 2013). NEDD8 conjugation is catalyzed by an E1 enzyme (NAE), two E2s (UBE2M and UBE2F), and several E3 enzymes (Zhao et al., 2014). Removal of NEDD8 is

catalyzed by the COP9 signalosome (CSN) and inactivates SCF (Cope and Deshaies, 2003; Cope et al., 2002; Enchev et al., 2012; Wei and Deng, 2003; Wolf et al., 2003). Intriguingly, although CSN inhibits SCF *in vitro* (Zhou et al., 2003), it is required for SCF activity *in vivo* (Cope and Deshaies, 2003). This apparent contradiction is often referred to as the CSN paradox. To reconcile this enigma, CSN-mediated ligase decommissioning has been proposed to orchestrate dynamic SR dismounting and reassembly (Cope and Deshaies, 2003; Schmidt et al., 2009; Wei and Deng, 2003; Wolf et al., 2003). In that model, only unneddylated CUL1 is available for subsequent SR exchange mediated by CAND1 (Liu et al., 2002; Zheng et al., 2002a). Additionally, CAND1 binding is instrumental to maintain a fraction of CUL1 backbones available for SR association (Reitsma et al., 2017). However, it remains unclear how these fundamental principles extend to other CRL families (Cavadini et al., 2016; Groisman et al., 2003; Mosadeghi et al., 2016). This is particularly relevant for CUL2- and CUL4-associated ligases, which are being harnessed for TPD.

Here, we map the genetic inventory required for ligand-induced targeted protein degradation. Our data suggest that resistance to degraders is predominantly defined by the nature of the hijacked CRL and not the degraded target. Moreover, our results support and contextualize the CSN paradox: although both act as negative regulators of SCF activity *in vitro*, we find them to be required for *in vivo* adaption to the CRL4-based, but not the CRL2-based, degraders tested. Mechanistically, we link the CSN paradox to a widespread auto-degradation of CRL SRs that is dynamically regulated in a cell-type-specific fashion. Collectively, our study highlights the relevance and subtleties of fundamental CRL regulatory circuits for the efficacy of a novel class of small-molecule therapeutics and informs on ligase-specific biomarkers and resistance mechanisms.

RESULTS

CRISPR/Cas9 Screens Identify Genetic Determinants of Targeted Protein Degradation

To identify global determinants of cellular sensitivity to small-molecule degraders, we performed genome-wide, positive-selection CRISPR/Cas9 knockout screens. To cover a broad target and E3 space, we compared five different degraders, including PROTACs (dBET6, THAL-SNS-032, and ARV-771) and molecular glues (indisulam and CC-885) that degrade different and overlapping substrates by harnessing $CRL4^{CRBN}$, $CRL4^{DCAF15}$, or $CRL2^{VHL}$ ligases (Han et al., 2017; Matyskiela et al., 2016; Olson et al., 2018; Raina et al., 2016; Uehara et al., 2017; Winter et al., 2017; Figure 1A). We thus aimed to distinguish common from ligase- or target-specific determinants of sensitivity. Screens were performed in the leukemia cell line KBM7 (Doench et al., 2016; Figure S1A). As expected, single guide RNAs (sgRNAs) targeting the hijacked substrate receptors (CRBN, DCAF15, and VHL) were enriched after treatment with the respective degrader (Figures 1A and S1B). Screens with CRBN-based dBET6, THAL-SNS-032, and CC-885 showed loss of UBE2G1 as a resistance mechanism, consistent with reports identifying UBE2G1 as the E2 ubiquitin-conjugating enzyme required for $CRL4^{CRBN}$ neomorphic substrates (Lu et al., 2018; Sievers et al., 2018a; Figure 1B). We also identify UBE2G1 to modulate indisulam sensitivity, suggesting that it similarly acts in destruction of $CRL4^{DCAF15}$ neosubstrates.

Generally, hits were enriched in processes involving CRL regulation, including the SR exchange factor CAND1 and the NEDD8-conjugating enzyme UBE2M (Figures 1C and S1C). Intriguingly, the COP9 signalosome (CSN) and associated deneddylation activity were exclusively identified for CRL4-modulating drugs but appeared inconsequential for ARV-771 reprogramming of $CRL2^{VHL}$ (Figures 1D and S1D). This is in line with recent data on the $CRL4^{CRBN}$-hijacking drug lenalidomide (Liu et al., 2019; Sievers et al., 2018a). Our identified gene-drug interactions manifested as a highly connected network when mapped on publicly available protein-protein interaction data (Alanis-Lobato et al., 2017; Figures 1E and S1E).

Network analysis segregated shared from drug-specific genetic requirements. Among others, we identified the E2 ligase UBE2R2 as a specific requirement for ARV-771 (Figure 1B). Conversely, integrator complex subunit INTS6 conferred sensitivity to CDK9 degradation, which is likely linked to target biology rather than impaired degradation (Baillat et al., 2005; Figure 1E). Network analysis highlighted multiple CSN components as shared dependencies of $CRL4^{CRBN}$- and $CRL4^{DCAF15}$-based degraders. Interestingly, sensitivity to the $CRL2^{VHL}$-based BET degrader ARV-771 was not linked to any CSN genes.

Collectively, intersection of five genome-scale CRISPR/Cas9 screens revealed shared and degrader-specific resistance factors. Our data imply that factors involved in CRL regulation outweigh target-specific resistance mechanisms. Importantly, these experiments suggest a differential and non-generalizable dependence of CRLs on CSN activity.

Key Determinants Functionally Converge on Impaired Target Protein Degradation

We selected 11 high-confidence hits for validation in competitive growth experiments (Table S1). Knockouts of all selected hits conferred resistance to the assayed degraders (Figures 2A and S2A). Five genes with strong sgRNA enrichment (UBE2M, CAND1, COPS1, COPS7B, and COPS8) were tested against all screened degraders (Figure S2B). Targeting of UBE2M conferred universal resistance to all tested degraders. In contrast, sgRNAs against CSN subunits or CAND1 selectively conveyed resistance against CRL4-based degraders, but not VHL-based ARV-771. Identified gene-drug interactions could be validated in additional cell lines (Figure S2C). Also in isolated loss-of-function (LOF) clones, UBE2M modulated efficacy of all degraders, and CAND1- and CSN-deficient cells were only resistant to CRL4-based compounds (Figures 2B, 2C, S2D, and S2E). No shifts in drug efficacy were observed for competitive antagonists of BET proteins (JQ1) and CDK9 (NVP-2; Figure S2F).

We next aimed to validate that identified resistances are due to impaired target protein degradation. Although CDK9 destabilization was compromised in all conditions, BRD4 degradation by $CRL2^{VHL}$-based ARV-771 was only abrogated in $UBE2M^{mut}$ cells (Figures 2D, S3A, and S3B). CRL-specific impairment of target degradation upon CSN perturbation could also be recapitulated pharmacologically (Schlierf et al., 2016; Figure 2E). Conversely,

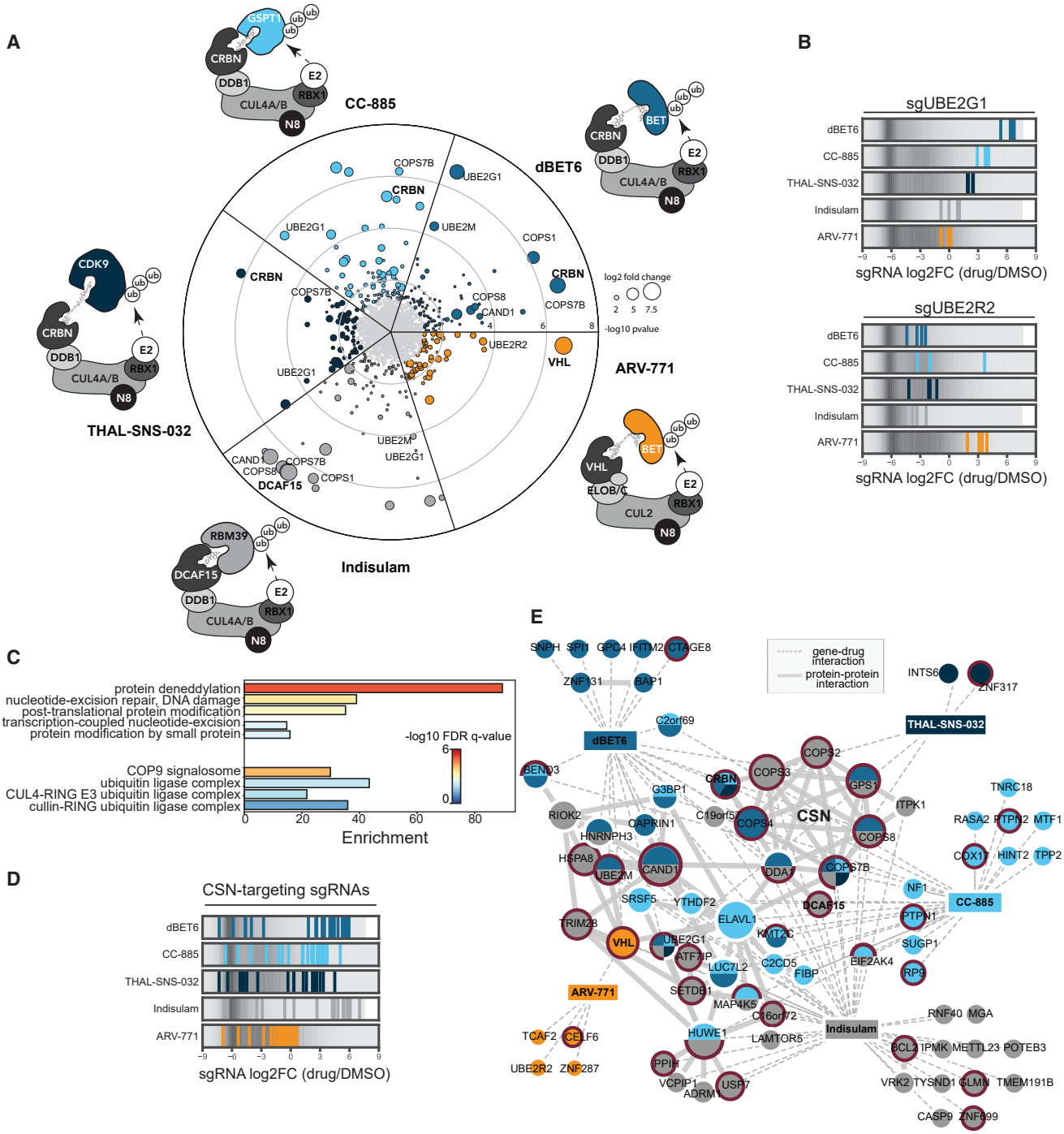

Figure 1. CRISPR/Cas9 Screens Identify Genetic Determinants of Targeted Protein Degradation

(A) Genome-wide, positive-selection CRISPR/Cas9 screens. Radial position indicates significance and circle size enrichment over control.

(B) Enrichment of sgRNAs targeting UBE2G1 and UBE2R2. Background represents the log2FC distribution of all sgRNAs in the respective screen.

(C) Gene Ontology (GO) terms enriched among all hits found in at least one screen (STARS q < 0.2).

(D) Enrichment of sgRNAs targeting CSN subunits identified as hits in at least one screen (COPS1, -2, -3, -4, -7B, and -8).

(E) Integrative network analysis distinguishes common from drug-specific hits. Significant hits were clustered by protein-protein (solid edges) and gene-drug interactions (dashed edges). Node colors indicate the different degrader screens. Node size correlates with connectivity. Strongest modulators (median sgRNA rank < 1,000) are highlighted in red.

See also Figure S1 and Table S1.

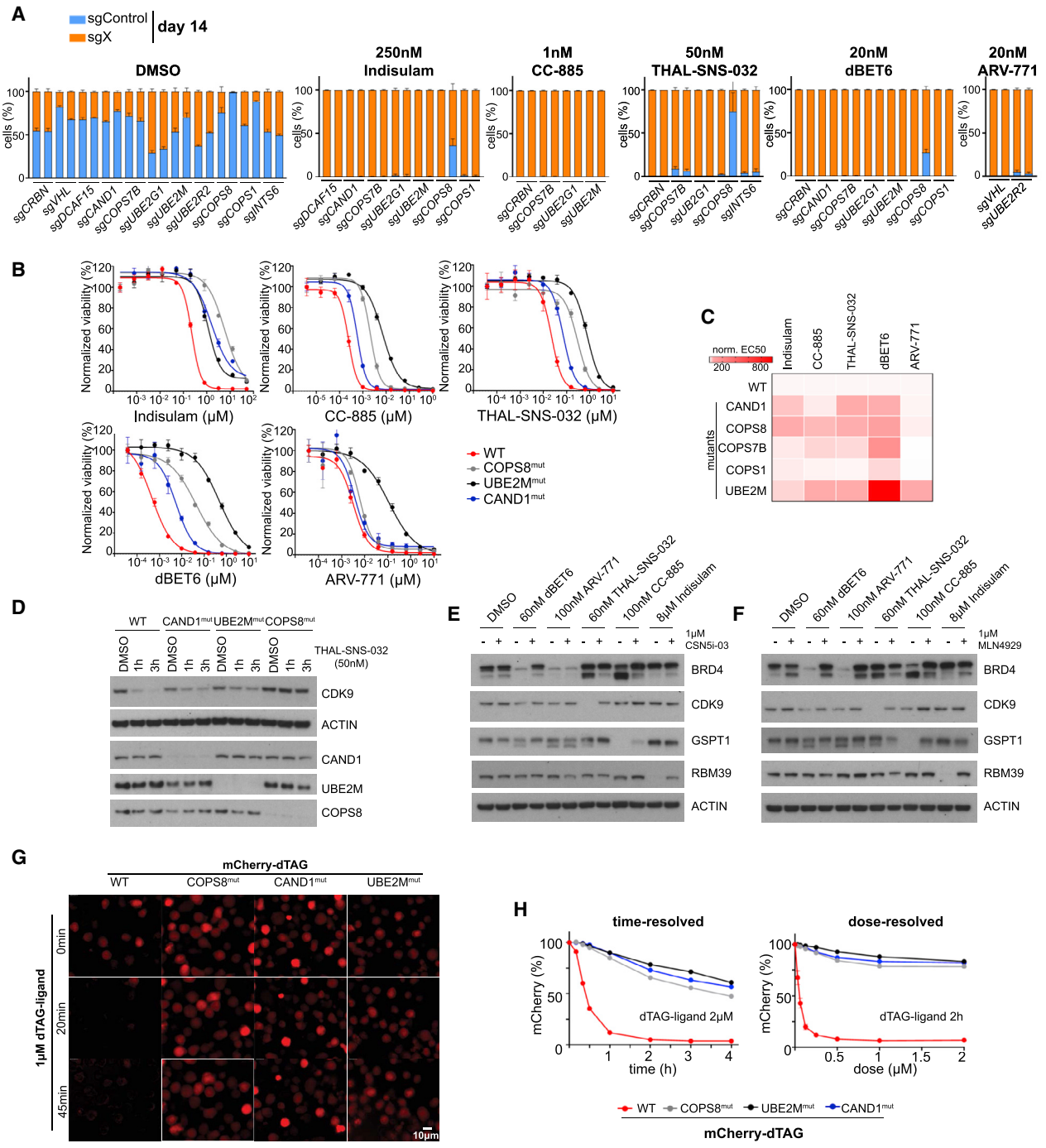

Figure 2. Loss of Cullin-RING Ligase Regulation Functionally Converges on Impaired Target Protein Degradation

(A) Competition growth experiments. Control cells (dTomato+) were mixed with EGFP+ cells transduced with sgRNAs against 11 selected hits. Pools were treated with the degrader(s) and flow cytometry quantified at days 0, 7 (see Figure S2A), and 14. Data points are averages of 3 replicates.

(B) DMSO-normalized viability in wild-type (WT) or LOF mutant KBM7 cells after 3-day treatments. Mean ± SEM; n = 3.

(C) EC_{50} fold changes in WT or LOF mutant KBM7 cells after 3-day treatments.

(D) CDK9 degradation upon exposure to THAL-SNS-032 in WT or LOF mutant KBM7 cells.

(E and F) Degradation efficiency of 5 h degrader treatment and (E) CSN5i-03 or (F) MLN4924.

(G) mCherry-dTAG degradation upon dTAG-ligand treatment in WT or LOF mutant KBM7.

(H) Flow cytometry-based analysis of degradation of mCherry-dTAG upon dTAG-ligand treatment in WT or LOF mutant KBM7 cells. Data points are averages of 3 replicates.

See also Figures S2 and S3, Video S1, and Table S1.

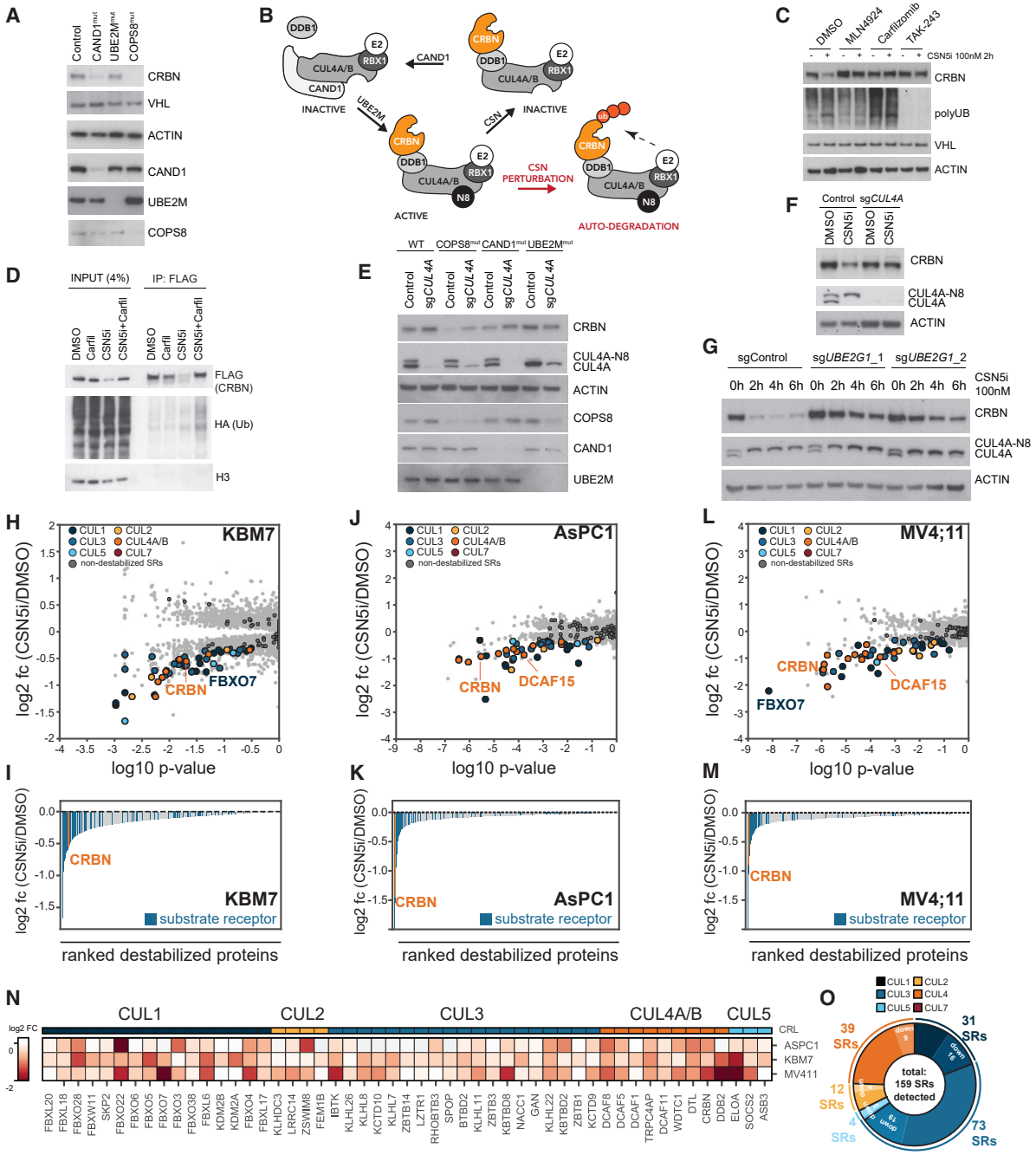

Figure 3. CAND1/CSN Perturbations Trigger CRBN Auto-degradation by Blocking CRL Decommissioning

(A) CRBN and VHL levels in CAND1^{mut}, UBE2M^{mut}, and COPS8^{mut} cells compared to control.

(B) Schematic of the CRL4^{CRBN} neddylation cycle. CSN perturbation traps CRL4^{CRBN} in a hyper-neddylated state, which induces CRBN auto-degradation.

(C) CSN5i-03 destabilizes CRBN. Pretreatment with 1 μM MLN4924, 1 μM carfilzomib, or 10 μM TAK-243 rescues auto-degradation.

(D) CSN5i-03 increases CRBN ubiquitination. FLAG-CRBN and hemagglutinin (HA)-Ub overexpressing 293T CRBN$^{-/-}$ cells were treated for 1 h with 1 μM carfilzomib and/or 2 μM CSN5i-03.

(E and F) Genetic CUL4A depletion reverts CRBN destabilization in COPS8^{mut} and CAND1^{mut} cells (E) and prevents CSN5i-mediated CRBN destabilization in WT cells (F).

(G) Genetic UBE2G1 depletion prevents CRBN destabilization by CSN5i-03 (2 h; 100 nM).

(H–M) Expression proteomics after CSN5i-03 treatment (1μM; 8 h).

(H, J, and L) SRs with log2FC < −0.3 in KBM7 (H), AsPC1 (J) and MV4;11 (L) cells are highlighted.Non-destabilized SRs are marked in dark gray.

(legend continued on next page)

the NAE inhibitor MLN4924 rescued effects of all degraders, recapitulating observations from UBE2M-deficient cells (Soucy et al., 2009; Figure 2F).

Finally, we aimed to extend our findings to an additional chemotype by deploying the degradation tag (dTAG) approach (Erb et al., 2017; Nabet et al., 2018). This strategy uses an $FKBP12^{F36V}$ tag to make fusion proteins amenable to ligand-induced protein degradation via $CRL4^{CRBN}$. We expressed mCherry-dTAG in the isolated LOF clones to visualize ligand-induced mCherry degradation. In all tested mutant backgrounds, mCherry degradation was abrogated compared to wild-type cells (Figures 2G, 2H, S3C, and S3D; Video S1).

CAND1/CSN Perturbations Trigger CRBN Auto-degradation by Blocking CRL Decommissioning

Next, we sought to determine the molecular mechanisms that diminish target proteolysis in degrader-resistant mutants. CUL2 and CUL4A neddylation in $UBE2M^{mut}$ cells was decreased to levels achieved by NAE inhibition in wild-type cells (Figure S4A). Resistance mechanisms via CAND1 and CSN inactivation appeared more intriguing, given that (1) they were ligase and/or context-dependent and (2) both are negative CRL regulators *in vitro*. In each initial screen, the strongest resistance emerged from direct SR knockout. We thus determined whether resistance of CAND1/COPS8 LOF mutants could similarly be explained by decreased SR abundance. Indeed, both $CAND1^{mut}$ and $COPS8^{mut}$ cells displayed significantly lower CRBN levels (Figure 3A). This is in line with previous findings that SCF ligases are destabilized after CSN inactivation via CSN5 knockdown (Cope and Deshaies, 2006). Selective CRBN destabilization could also be recapitulated by pharmacologic CSN inhibition (Figures S4B–S4D). Conversely, levels of the CRL2 SR VHL were unchanged in either of the mutant backgrounds (Figure 3A).

Given that CSN and CAND1 maintain the plasticity of the cellular CRL repertoire, we aimed to explain how an imbalanced CRL4 repertoire leads to decreased CRBN abundance. Of note, a recent study linked CRBN destabilization upon CSN perturbation to increased activity of the SCF ligase FBXO7 (Liu et al., 2019). Here, we propose that loss of CAND1/CSN locks $CRL4^{CRBN}$ in a constitutively active state by abolishing CRL4 decommissioning. In the absence of CRBN-bound substrate, constitutive activity would thus cause auto-degradation when CRBN is positioned in the CRL4 ubiquitination zone (Figure 3B). Supporting our hypothesis, SR auto-degradation has been described for yeast SCF ligases (Galan and Peter, 1999; Zhou and Howley, 1998). In such a model, we would expect CRBN destabilization to be (1) dependent on $CRL4^{CRBN}$ co-factors, (2) not restricted to CRBN but affecting other SRs, and (3) reversible upon induced substrate availability (Li et al., 2004).

Consistent with expectation (1), CSN5i-mediated CRBN destabilization was rescued by inhibition of NAE, UBA1, or the proteasome (Figure 3C). Moreover, CSN inhibition triggered CRBN poly-ubiquitination (Figure 3D). CUL4A depletion also reverted CRBN destabilization in $COPS8^{mut}$ and $CAND1^{mut}$ cells (Figure 3E). Similarly, CUL4A or UBE2G1 ablation prevented CSN5i-driven CRBN destabilization (Figures 3F and 3G).

Auto-degradation after CSN Perturbation Affects a Wide Spectrum of Substrate Receptors

Next, we charted whether other SRs similarly depend on CRL decommissioning by CAND1/CSN. Quantitative proteomics after CSN inhibition in KBM7 cells revealed widespread destabilization of SRs from all cullin classes, including CRBN (Figures 3H and 3I; STAR Methods; Tables S2 and S3). In fact, SRs were among the strongest downregulated proteins (Figure 3I). CRBN destabilization, along with globally decreased SR abundance, was also detected in $COPS8^{mut}$ and, less pronounced, $CAND1^{mut}$ cells (Figures S4E and S4F). The dependence of CRBN and other SRs on the CSN was conserved in other cellular backgrounds (Figures 3J–3M and S4G). Intriguingly, CSN dependence of a given SR appeared highly context specific, as several SRs were only destabilized in particular cellular backgrounds. Examples are the CUL3-associated KBTBD8, the CUL2-associated ZSWIM8, or the CUL1-associated KDM2A (Figures 3N and S4H). CSN dependence was not correlated to SR abundance (Figures S4I and S4J). Moreover, levels of many SRs were not changed by CSN inhibition (Figure 3O). Unexpectedly, we also detected destabilization of FBXO7 in two cellular backgrounds. This suggests that, at least in these cell lines, CRBN destabilization is likely not directly caused by increased $CRL1^{FBXO7}$ activity as previously proposed (Liu et al., 2019). In summary, we provide a comprehensive assessment of cullin-associated SRs that are destabilized upon CAND1/CSN inactivation. Our data link resistance via abrogated CRL plasticity to auto-degradation of numerous SRs, including CRBN. Although CRBN was destabilized in all assayed cell types, CSN dependence of other SRs was highly context and cell line specific.

Drug-Induced Neosubstrate Recruitment Reverts Auto-degradation

We next tested whether neosubstrate could protect SRs from auto-degradation. Indeed, GSPT1 recruitment to $CRL4^{CRBN}$ by CC-885 decreased subsequent CSNi-mediated CRBN destabilization (Figures 4A and 4B). Substrate binding also reversed an already destabilized state, as chemical CDK9 recruitment after CSN inhibition re-stabilized CRBN in a time-dependent manner (Figure 4C). Similar re-stabilization was observed after BET protein or GSPT1 recruitment (Figures S5A and S5B). Also in $COPS8^{mut}$ cells, CRBN destabilization was reverted by CC-885 treatment (Figure S5C). Together, we found that ligand-induced neosubstrate recruitment prevents and counteracts CRBN auto-degradation in CSN-perturbed conditions. This suggests that loss of SR abundance via auto-degradation might not fully explain the observed drug resistance. We hence decided to address whether CSN perturbations also affect drug-induced substrate recruitment. To circumvent post-lysis CRL

(I, K, and M) All destabilized proteins in KBM7 (I), AsPC1 (K) and MV4;11 (M) cells. SRs are highlighted in blue and CRBN in orange.
(N) Log2FCs of all SRs destabilized by CSN5i-03 in at least one cell line (log2FC < −0.3).
(O) All SRs detected in at least one cell line grouped by predicted cullin association and destabilization upon CSN inhibition.
See also Figure S4 and Tables S2 and S3.

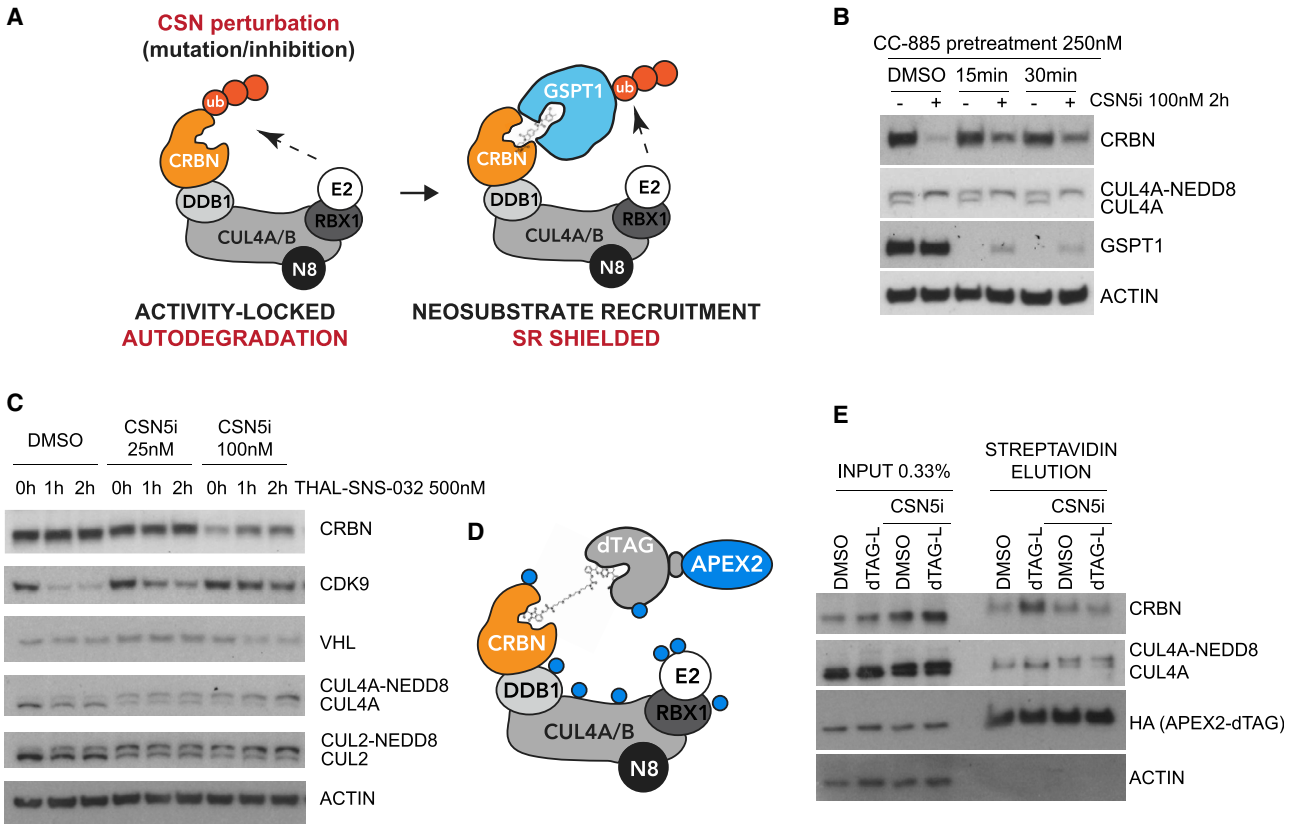

Figure 4. Degrader Treatment Reverts Auto-degradation, and Acute CSN Inhibition Impairs CRL Dynamics

(A) Model how degrader treatment could rescue SR auto-degradation. Degrader-induced neosubstrate recruitment shields the SR from ubiquitin transfer.

(B) CC-885 pretreatment counteracts CSN5i-triggered CRBN destabilization in KBM7 WT cells.

(C) Pretreatment with CSN5i-03 before THAL-SNS-032 similarly reverts CRBN destabilization.

(D) APEX2-dTAG proximity labeling to assess drug-induced remodeling of CRL complexes in intact cells.

(E) Enrichment of biotin-labeled CUL4A and CRBN following pulsed dTAG-ligand treatment (1 μM; 5 min) in CSN5i-03 (1 μM; 20 min) pretreated cells.

See also Figure S5.

composition changes (Reitsma et al., 2017), we employed APEX2 proximity labeling *in situ* (Rhee et al., 2013). Ectopic expression of APEX2-dTAG allowed us to monitor the dynamics of ligand-induced substrate recruitment to $CRL4^{CRBN}$ (Figure 4D). Acute CSN inhibition permitted measurements prior to CRBN destabilization (Figures 4E, S4D, and S5D). We confirmed that ligand treatment recruited APEX2-dTAG to CRBN and CUL4A in unperturbed conditions (Figure 4E). Interestingly, CSN inhibition profoundly impaired APEX2-dTAG incorporation into a mature $CRL4^{CRBN}$ complex, indicating that CSN activity is required for substrate-driven CRL assembly. We conclude that impaired neddylation affects the response to small-molecule degraders not only via SR auto-degradation but also by abrogating CRL plasticity downstream of neosubstrate availability.

DISCUSSION

Ligand-induced targeted protein degradation (TPD) resets many concepts of traditional pharmacology. A unique feature of small-molecule degraders is that they act catalytically. Conceivably, cellular response to TPD needs to sustain catalytic drug action. Here, we set out to map the cellular determinants of TPD. Identification of the CAND1/CSN axis as a major resistance driver is consistent with a conundrum known as the CSN paradox. Our findings support that both components are required for cellular CRL activity despite being negative CRL regulators *in vitro*. Of note, most research on the CSN paradox and overall CRL regulation stems from work on SCF ligases. Our work suggests that principles of SCF regulation likely extend to many CRLs. Intriguingly, our data show that the dependence of CRLs on the CAND1/CSN axis can be highly context specific. Effectors required for drug-induced proteolysis not only depended on the hijacked CRL but also on the cellular background. Although drugs harnessing $CRL4^{CRBN}$ or $CRL4^{DCAF15}$ depended on CAND1/CSN, efficacy of $CRL2^{VHL}$-based ARV-771 did not rely on this axis in the tested cellular models. Previous studies implicated $CRL1^{FBXO7}$ in CSN-dependent destabilization of CRBN (Liu et al., 2019). In the leukemia cell lines assayed here, we find FBXO7 itself among the most destabilized SR. Although our data do not exclude a direct contribution of FBXO7 to CRBN destabilization, we conclude

that a model of widespread SR auto-degradation is most consistent with our observations.

Mechanistically, the requirement of small-molecule degraders on the CAND1/CSN axis manifested two-fold. First, acute CSN inhibition affected the dynamics of drug-induced CRL assembly. Second, auto-degradation of several CRL SRs abrogated degrader efficacy. Further research will be required to understand what sensitizes SRs to auto-degradation. Biophysical characteristics, such as affinity of the SR and adaptor dimer to the cullin scaffold or spatial positioning of the SR in the E2 ubiquitination zone, could contribute but presumably fail to account for the observed context dependency (Cavadini et al., 2016; Fischer et al., 2011; Lingaraju et al., 2014; Liu et al., 2018; Mosadeghi et al., 2016). A causative role of SR abundance was also ruled out by correlative analysis of the assayed cell types. Instead, we observed that drug-induced neosubstrate recruitment transiently protected an otherwise auto-degrading SR. Hence, we envision that substrate occupancy of a given SR could influence its susceptibility to auto-degradation. Collectively, our data outline cell-specific differences in CAND1/CSN dependency, point to an explanation for differential degrader efficacy in distinct cellular backgrounds, and inform on possible resistance mechanisms for upcoming clinical studies (Winter et al., 2017; Zorba et al., 2018).

STAR★METHODS

Detailed methods are provided in the online version of this paper and include the following:

- KEY RESOURCES TABLE
- LEAD CONTACT AND MATERIALS AVAILABILITY
- EXPERIMENTAL MODEL AND SUBJECT DETAILS
  - Cell lines
- METHOD DETAILS
  - Brunello lentivirus production
  - Brunello pooled library screens
  - Library preparation for next generation sequencing
  - Next generation sequencing data analysis
  - Interactome construction
  - Gene Ontology enrichment analysis
  - Competition growth experiments
  - Isolation and characterization of single mutant clones
  - Cell viability assays
  - Western blot analysis
  - Drug treatments for target degradation assessment
  - mCherry-dTAG reporter: live cell imaging and flow cytometry
  - Substrate receptor auto-degradation
  - CRBN ubiquitination
  - Immunoprecipitation
  - Lists of putative substrate receptors associated to each cullin
  - Expression proteomics
  - Drug treatments for ligand-mediated CRBN re-stabilization and protection from CRBN auto-degradation
  - APEX2-dTAG experiments
- QUANTIFICATION AND STATISTICAL ANALYSIS
- DATA AND CODE AVAILABILITY

SUPPLEMENTAL INFORMATION

Supplemental Information can be found online at https://doi.org/10.1016/j.molcel.2019.07.013.

ACKNOWLEDGMENTS

We thank N.S. Gray for providing THAL-SNS-032 and dBET6. We thank F. Bassermann for kindly sharing CRBN antibody. CeMM and the Winter lab are supported by the Austrian Academy of Sciences. C.M.-R. is supported by an EMBO-LT fellowship (EMBO-LTF ALTF 676-2017). M.G.J. is supported by a Boehringer Ingelheim Fonds PhD fellowship. Sequencing was performed at the Biomedical Sequencing facility and proteomics at the Proteomics facility at CeMM. Microscopy was performed at the imaging core facility of the Medical University of Vienna.

AUTHOR CONTRIBUTIONS

C.M.-R. analyzed data, made figures, and performed experiments, including western blots, drug-sensitivity assays, microscopy, fluorescence-activated cell sorting (FACS), APEX, and proteomics sample preparation. M.G.J. conducted CRISPR screens and analyzed data. S.B. performed immunoblots, drug-sensitivity assays, and provided technical help in additional experiments. M.B. analyzed CRISPR screens and made figures. C.S. performed network analysis. A.H. analyzed proteomics data. A.C.M. performed tandem mass tag (TMT) labeling and analyzed proteomics data. J.M. supervised network analysis. C.M.-R., M.G.J., and G.E.W. wrote the manuscript. G.E.W. has planned and supervised the presented research and has overall project responsibility.

DECLARATION OF INTERESTS

A patent covering CRL dynamics published in this manuscript has been filed.

Received: April 2, 2019
Revised: June 13, 2019
Accepted: July 9, 2019
Published: August 22, 2019

REFERENCES

Alanis-Lobato, G., Andrade-Navarro, M.A., and Schaefer, M.H. (2017). HIPPIE v2.0: enhancing meaningfulness and reliability of protein-protein interaction networks. Nucleic Acids Res. *45* (D1), D408–D414.

Baillat, D., Hakimi, M.A., Näär, A.M., Shilatifard, A., Cooch, N., and Shiekhattar, R. (2005). Integrator, a multiprotein mediator of small nuclear RNA processing, associates with the C-terminal repeat of RNA polymerase II. Cell *123*, 265–276.

Bondeson, D.P., Mares, A., Smith, I.E., Ko, E., Campos, S., Miah, A.H., Mulholland, K.E., Routly, N., Buckley, D.L., Gustafson, J.L., et al. (2015). Catalytic in vivo protein knockdown by small-molecule PROTACs. Nat. Chem. Biol. *11*, 611–617.

Braschi, B., Denny, P., Gray, K., Jones, T., Seal, R., Tweedie, S., Yates, B., and Bruford, E. (2019). Genenames.org: the HGNC and VGNC resources in 2019. Nucleic Acids Res *47*, D786–D792.

Carette, J.E., Guimaraes, C.P., Varadarajan, M., Park, A.S., Wuethrich, I., Godarova, A., Kotecki, M., Cochran, B.H., Spooner, E., Ploegh, H.L., and Brummelkamp, T.R. (2009). Haploid genetic screens in human cells identify host factors used by pathogens. Science *326*, 1231–1235.

Cavadini, S., Fischer, E.S., Bunker, R.D., Potenza, A., Lingaraju, G.M., Goldie, K.N., Mohamed, W.I., Faty, M., Petzold, G., Beckwith, R.E., et al. (2016). Cullin-RING ubiquitin E3 ligase regulation by the COP9 signalosome. Nature *531*, 598–603.

Chevrier, S., and Corcoran, L.M. (2014). BTB-ZF transcription factors, a growing family of regulators of early and late B-cell development. Immunol. Cell Biol. *92*, 481–488.

Cope, G.A., and Deshaies, R.J. (2003). COP9 signalosome: a multifunctional regulator of SCF and other cullin-based ubiquitin ligases. Cell *114*, 663–671.

Cope, G.A., and Deshaies, R.J. (2006). Targeted silencing of Jab1/Csn5 in human cells downregulates SCF activity through reduction of F-box protein levels. BMC Biochem. *7*, 1.

Cope, G.A., Suh, G.S., Aravind, L., Schwarz, S.E., Zipursky, S.L., Koonin, E.V., and Deshaies, R.J. (2002). Role of predicted metalloprotease motif of Jab1/Csn5 in cleavage of Nedd8 from Cul1. Science *298*, 608–611.

Deshaies, R.J., Emberley, E.D., and Saha, A. (2010). Control of cullin-ring ubiquitin ligase activity by nedd8. Subcell. Biochem. *54*, 41–56.

Dias, D.C., Dolios, G., Wang, R., and Pan, Z.Q. (2002). CUL7: a DOC domain-containing cullin selectively binds Skp1.Fbx29 to form an SCF-like complex. Proc. Natl. Acad. Sci. USA *99*, 16601–16606.

Doench, J.G., Fusi, N., Sullender, M., Hegde, M., Vaimberg, E.W., Donovan, K.F., Smith, I., Tothova, Z., Wilen, C., Orchard, R., et al. (2016). Optimized sgRNA design to maximize activity and minimize off-target effects of CRISPR-Cas9. Nat. Biotechnol. *34*, 184–191.

Dubiel, W., Dubiel, D., Wolf, D.A., and Naumann, M. (2018). Cullin 3-based ubiquitin ligases as master regulators of mammalian cell differentiation. Trends Biochem. Sci. *43*, 95–107.

Eden, E., Navon, R., Steinfeld, I., Lipson, D., and Yakhini, Z. (2009). GOrilla: a tool for discovery and visualization of enriched GO terms in ranked gene lists. BMC Bioinformatics *10*, 48.

Eichner, R., Heider, M., Fernández-Sáiz, V., van Bebber, F., Garz, A.K., Lemeer, S., Rudelius, M., Targosz, B.S., Jacobs, L., Knorn, A.M., et al. (2016). Immunomodulatory drugs disrupt the cereblon-CD147-MCT1 axis to exert antitumor activity and teratogenicity. Nat. Med. *22*, 735–743.

Enchev, R.I., Scott, D.C., da Fonseca, P.C., Schreiber, A., Monda, J.K., Schulman, B.A., Peter, M., and Morris, E.P. (2012). Structural basis for a reciprocal regulation between SCF and CSN. Cell Rep. *2*, 616–627.

Erb, M.A., Scott, T.G., Li, B.E., Xie, H., Paulk, J., Seo, H.S., Souza, A., Roberts, J.M., Dastjerdi, S., Buckley, D.L., et al. (2017). Transcription control by the ENL YEATS domain in acute leukaemia. Nature *543*, 270–274.

Fischer, E.S., Scrima, A., Böhm, K., Matsumoto, S., Lingaraju, G.M., Faty, M., Yasuda, T., Cavadini, S., Wakasugi, M., Hanaoka, F., et al. (2011). The molecular basis of CRL4DDB2/CSA ubiquitin ligase architecture, targeting, and activation. Cell *147*, 1024–1039.

Gadd, M.S., Testa, A., Lucas, X., Chan, K.H., Chen, W., Lamont, D.J., Zengerle, M., and Ciulli, A. (2017). Structural basis of PROTAC cooperative recognition for selective protein degradation. Nat. Chem. Biol. *13*, 514–521.

Galan, J.M., and Peter, M. (1999). Ubiquitin-dependent degradation of multiple F-box proteins by an autocatalytic mechanism. Proc. Natl. Acad. Sci. USA *96*, 9124–9129.

Ghiassian, S.D., Menche, J., and Barabási, A.L. (2015). A DIseAse MOdule Detection (DIAMOnD) algorithm derived from a systematic analysis of connectivity patterns of disease proteins in the human interactome. PLoS Comput. Biol. *11*, e1004120.

Gilar, M., Olivova, P., Daly, A.E., and Gebler, J.C. (2005). Two-dimensional separation of peptides using RP-RP-HPLC system with different pH in first and second separation dimensions. J. Sep. Sci. *28*, 1694–1703.

Groisman, R., Polanowska, J., Kuraoka, I., Sawada, J., Saijo, M., Drapkin, R., Kisselev, A.F., Tanaka, K., and Nakatani, Y. (2003). The ubiquitin ligase activity in the DDB2 and CSA complexes is differentially regulated by the COP9 signalosome in response to DNA damage. Cell *113*, 357–367.

Han, T., Goralski, M., Gaskill, N., Capota, E., Kim, J., Ting, T.C., Xie, Y., Williams, N.S., and Nijhawan, D. (2017). Anticancer sulfonamides target splicing by inducing RBM39 degradation via recruitment to DCAF15. Science *356*, eaal3755.

He, Y.J., McCall, C.M., Hu, J., Zeng, Y., and Xiong, Y. (2006). DDB1 functions as a linker to recruit receptor WD40 proteins to CUL4-ROC1 ubiquitin ligases. Genes Dev. *20*, 2949–2954.

Hershko, A., Ciechanover, A., and Varshavsky, A. (2000). Basic Medical Research Award. The ubiquitin system. Nat. Med. *6*, 1073–1081.

Hung, V., Udeshi, N.D., Lam, S.S., Loh, K.H., Cox, K.J., Pedram, K., Carr, S.A., and Ting, A.Y. (2016). Spatially resolved proteomic mapping in living cells with the engineered peroxidase APEX2. Nat. Protoc. *11*, 456–475.

Ito, T., Ando, H., Suzuki, T., Ogura, T., Hotta, K., Imamura, Y., Yamaguchi, Y., and Handa, H. (2010). Identification of a primary target of thalidomide teratogenicity. Science *327*, 1345–1350.

Jin, J., Cardozo, T., Lovering, R.C., Elledge, S.J., Pagano, M., and Harper, J.W. (2004). Systematic analysis and nomenclature of mammalian F-box proteins. Genes Dev. *18*, 2573–2580.

Kamura, T., Maenaka, K., Kotoshiba, S., Matsumoto, M., Kohda, D., Conaway, R.C., Conaway, J.W., and Nakayama, K.I. (2004). VHL-box and SOCS-box domains determine binding specificity for Cul2-Rbx1 and Cul5-Rbx2 modules of ubiquitin ligases. Genes Dev. *18*, 3055–3065.

Komander, D., and Rape, M. (2012). The ubiquitin code. Annu. Rev. Biochem. *81*, 203–229.

Krönke, J., Udeshi, N.D., Narla, A., Grauman, P., Hurst, S.N., McConkey, M., Svinkina, T., Heckl, D., Comer, E., Li, X., et al. (2014). Lenalidomide causes selective degradation of IKZF1 and IKZF3 in multiple myeloma cells. Science *343*, 301–305.

Langmead, B., and Salzberg, S.L. (2012). Fast gapped-read alignment with Bowtie 2. Nat. Methods *9*, 357–359.

Lee, J., and Zhou, P. (2007). DCAFs, the missing link of the CUL4-DDB1 ubiquitin ligase. Mol. Cell *26*, 775–780.

Li, Y., Gazdoiu, S., Pan, Z.Q., and Fuchs, S.Y. (2004). Stability of homologue of Slimb F-box protein is regulated by availability of its substrate. J. Biol. Chem. *279*, 11074–11080.

Lingaraju, G.M., Bunker, R.D., Cavadini, S., Hess, D., Hassiepen, U., Renatus, M., Fischer, E.S., and Thomä, N.H. (2014). Crystal structure of the human COP9 signalosome. Nature *512*, 161–165.

Liu, J., Furukawa, M., Matsumoto, T., and Xiong, Y. (2002). NEDD8 modification of CUL1 dissociates p120(CAND1), an inhibitor of CUL1-SKP1 binding and SCF ligases. Mol. Cell *10*, 1511–1518.

Liu, X., Reitsma, J.M., Mamrosh, J.L., Zhang, Y., Straube, R., and Deshaies, R.J. (2018). Cand1-mediated adaptive exchange mechanism enables variation in F-box protein expression. Mol. Cell *69*, 773–786.e6.

Liu, J., Song, T., Zhou, W., Xing, L., Wang, S., Ho, M., Peng, Z., Tai, Y.T., Hideshima, T., Anderson, K.C., and Cang, Y. (2019). A genome-scale CRISPR-Cas9 screening in myeloma cells identifies regulators of immunomodulatory drug sensitivity. Leukemia *33*, 171–180.

Lu, G., Middleton, R.E., Sun, H., Naniong, M., Ott, C.J., Mitsiades, C.S., Wong, K.K., Bradner, J.E., and Kaelin, W.G., Jr. (2014). The myeloma drug lenalidomide promotes the cereblon-dependent destruction of Ikaros proteins. Science *343*, 305–309.

Lu, J., Qian, Y., Altieri, M., Dong, H., Wang, J., Raina, K., Hines, J., Winkler, J.D., Crew, A.P., Coleman, K., and Crews, C.M. (2015). Hijacking the E3 ubiquitin ligase cereblon to efficiently target BRD4. Chem. Biol. *22*, 755–763.

Lu, G., Weng, S., Matyskiela, M., Zheng, X., Fang, W., Wood, S., Surka, C., Mizukoshi, R., Lu, C.C., Mendy, D., et al. (2018). UBE2G1 governs the destruction of cereblon neomorphic substrates. eLife *7*, e40958.

Mahrour, N., Redwine, W.B., Florens, L., Swanson, S.K., Martin-Brown, S., Bradford, W.D., Staehling-Hampton, K., Washburn, M.P., Conaway, R.C., and Conaway, J.W. (2008). Characterization of Cullin-box sequences that direct recruitment of Cul2-Rbx1 and Cul5-Rbx2 modules to Elongin BC-based ubiquitin ligases. J. Biol. Chem. *283*, 8005–8013.

Martin, M. (2011). Cutadapt removes adapter sequences from high-throughput sequencing reads. EMBnet.journal *17*, 3.

Matyskiela, M.E., Lu, G., Ito, T., Pagarigan, B., Lu, C.C., Miller, K., Fang, W., Wang, N.Y., Nguyen, D., Houston, J., et al. (2016). A novel cereblon modulator recruits GSPT1 to the CRL4(CRBN) ubiquitin ligase. Nature *535*, 252–257.

Mosadeghi, R., Reichermeier, K.M., Winkler, M., Schreiber, A., Reitsma, J.M., Zhang, Y., Stengel, F., Cao, J., Kim, M., Sweredoski, M.J., et al. (2016). Structural and kinetic analysis of the COP9-Signalosome activation and the cullin-RING ubiquitin ligase deneddylation cycle. eLife *5*, e12102.

Nabet, B., Roberts, J.M., Buckley, D.L., Paulk, J., Dastjerdi, S., Yang, A., Leggett, A.L., Erb, M.A., Lawlor, M.A., Souza, A., et al. (2018). The dTAG system for immediate and target-specific protein degradation. Nat. Chem. Biol. *14*, 431–441.

Nowak, R.P., DeAngelo, S.L., Buckley, D., He, Z., Donovan, K.A., An, J., Safaee, N., Jedrychowski, M.P., Ponthier, C.M., Ishoey, M., et al. (2018). Plasticity in binding confers selectivity in ligand-induced protein degradation. Nat. Chem. Biol. *14*, 706–714.

Olson, C.M., Jiang, B., Erb, M.A., Liang, Y., Doctor, Z.M., Zhang, Z., Zhang, T., Kwiatkowski, N., Boukhali, M., Green, J.L., et al. (2018). Pharmacological perturbation of CDK9 using selective CDK9 inhibition or degradation. Nat. Chem. Biol. *14*, 163–170.

Petzold, G., Fischer, E.S., and Thomä, N.H. (2016). Structural basis of lenalidomide-induced CK1α degradation by the CRL4(CRBN) ubiquitin ligase. Nature *532*, 127–130.

Pierce, N.W., Lee, J.E., Liu, X., Sweredoski, M.J., Graham, R.L., Larimore, E.A., Rome, M., Zheng, N., Clurman, B.E., Hess, S., et al. (2013). Cand1 promotes assembly of new SCF complexes through dynamic exchange of F box proteins. Cell *153*, 206–215.

Pintard, L., Willems, A., and Peter, M. (2004). Cullin-based ubiquitin ligases: Cul3-BTB complexes join the family. EMBO J. *23*, 1681–1687.

Raina, K., Lu, J., Qian, Y., Altieri, M., Gordon, D., Rossi, A.M., Wang, J., Chen, X., Dong, H., Siu, K., et al. (2016). PROTAC-induced BET protein degradation as a therapy for castration-resistant prostate cancer. Proc. Natl. Acad. Sci. USA *113*, 7124–7129.

Reitsma, J.M., Liu, X., Reichermeier, K.M., Moradian, A., Sweredoski, M.J., Hess, S., and Deshaies, R.J. (2017). Composition and regulation of the cellular repertoire of SCF ubiquitin ligases. Cell *171*, 1326–1339.e14.

Rhee, H.W., Zou, P., Udeshi, N.D., Martell, J.D., Mootha, V.K., Carr, S.A., and Ting, A.Y. (2013). Proteomic mapping of mitochondria in living cells via spatially restricted enzymatic tagging. Science *339*, 1328–1331.

Roy, M.J., Winkler, S., Hughes, S.J., Whitworth, C., Galant, M., Farnaby, W., Rumpel, K., and Ciulli, A. (2019). SPR-measured dissociation kinetics of PROTAC ternary complexes influence target degradation rate. ACS Chem. Biol. *14*, 361–368.

Sakamoto, K.M., Kim, K.B., Kumagai, A., Mercurio, F., Crews, C.M., and Deshaies, R.J. (2001). Protacs: chimeric molecules that target proteins to the Skp1-Cullin-F box complex for ubiquitination and degradation. Proc. Natl. Acad. Sci. USA *98*, 8554–8559.

Schlierf, A., Altmann, E., Quancard, J., Jefferson, A.B., Assenberg, R., Renatus, M., Jones, M., Hassiepen, U., Schaefer, M., Kiffe, M., et al. (2016). Targeted inhibition of the COP9 signalosome for treatment of cancer. Nat. Commun. *7*, 13166.

Schmidt, M.W., McQuary, P.R., Wee, S., Hofmann, K., and Wolf, D.A. (2009). F-box-directed CRL complex assembly and regulation by the CSN and CAND1. Mol. Cell *35*, 586–597.

Sievers, Q.L., Gasser, J.A., Cowley, G.S., Fischer, E.S., and Ebert, B.L. (2018a). Genome-wide screen identifies cullin-RING ligase machinery required for lenalidomide-dependent $CRL4^{CRBN}$ activity. Blood *132*, 1293–1303.

Sievers, Q.L., Petzold, G., Bunker, R.D., Renneville, A., Słabicki, M., Liddicoat, B.J., Abdulrahman, W., Mikkelsen, T., Ebert, B.L., and Thomä, N.H. (2018b). Defining the human C2H2 zinc finger degrome targeted by thalidomide analogs through CRBN. Science *362*, eaat0572.

Silva, J.C., Gorenstein, M.V., Li, G.Z., Vissers, J.P., and Geromanos, S.J. (2006). Absolute quantification of proteins by LCMSE: a virtue of parallel MS acquisition. Mol. Cell. Proteomics *5*, 144–156.

Soucy, T.A., Smith, P.G., Milhollen, M.A., Berger, A.J., Gavin, J.M., Adhikari, S., Brownell, J.E., Burke, K.E., Cardin, D.P., Critchley, S., et al. (2009). An inhibitor of NEDD8-activating enzyme as a new approach to treat cancer. Nature *458*, 732–736.

Stogios, P.J., Downs, G.S., Jauhal, J.J., Nandra, S.K., and Privé, G.G. (2005). Sequence and structural analysis of BTB domain proteins. Genome Biol. *6*, R82.

Uehara, T., Minoshima, Y., Sagane, K., Sugi, N.H., Mitsuhashi, K.O., Yamamoto, N., Kamiyama, H., Takahashi, K., Kotake, Y., Uesugi, M., et al. (2017). Selective degradation of splicing factor CAPERα by anticancer sulfonamides. Nat. Chem. Biol. *13*, 675–680.

Wang, Y., Yang, F., Gritsenko, M.A., Wang, Y., Clauss, T., Liu, T., Shen, Y., Monroe, M.E., Lopez-Ferrer, D., Reno, T., et al. (2011). Reversed-phase chromatography with multiple fraction concatenation strategy for proteome profiling of human MCF10A cells. Proteomics *11*, 2019–2026.

Wei, N., and Deng, X.W. (2003). The COP9 signalosome. Annu. Rev. Cell Dev. Biol. *19*, 261–286.

Winter, G.E., Buckley, D.L., Paulk, J., Roberts, J.M., Souza, A., Dhe-Paganon, S., and Bradner, J.E. (2015). DRUG DEVELOPMENT. Phthalimide conjugation as a strategy for in vivo target protein degradation. Science *348*, 1376–1381.

Winter, G.E., Mayer, A., Buckley, D.L., Erb, M.A., Roderick, J.E., Vittori, S., Reyes, J.M., di Iulio, J., Souza, A., Ott, C.J., et al. (2017). BET bromodomain proteins function as master transcription elongation factors independent of CDK9 recruitment. Mol. Cell *67*, 5–18.e19.

Wiśniewski, J.R., Zougman, A., Nagaraj, N., and Mann, M. (2009). Universal sample preparation method for proteome analysis. Nat. Methods *6*, 359–362.

Wolf, D.A., Zhou, C., and Wee, S. (2003). The COP9 signalosome: an assembly and maintenance platform for cullin ubiquitin ligases? Nat. Cell Biol. *5*, 1029–1033.

Zengerle, M., Chan, K.H., and Ciulli, A. (2015). Selective small molecule induced degradation of the BET bromodomain protein BRD4. ACS Chem. Biol. *10*, 1770–1777.

Zhao, Y., Morgan, M.A., and Sun, Y. (2014). Targeting Neddylation pathways to inactivate cullin-RING ligases for anticancer therapy. Antioxid. Redox Signal. *21*, 2383–2400.

Zheng, J., Yang, X., Harrell, J.M., Ryzhikov, S., Shim, E.H., Lykke-Andersen, K., Wei, N., Sun, H., Kobayashi, R., and Zhang, H. (2002a). CAND1 binds to unneddylated CUL1 and regulates the formation of SCF ubiquitin E3 ligase complex. Mol. Cell *10*, 1519–1526.

Zheng, N., Schulman, B.A., Song, L., Miller, J.J., Jeffrey, P.D., Wang, P., Chu, C., Koepp, D.M., Elledge, S.J., Pagano, M., et al. (2002b). Structure of the Cul1-Rbx1-Skp1-F boxSkp2 SCF ubiquitin ligase complex. Nature *416*, 703–709.

Zhou, P., and Howley, P.M. (1998). Ubiquitination and degradation of the substrate recognition subunits of SCF ubiquitin-protein ligases. Mol. Cell *2*, 571–580.

Zhou, C., Wee, S., Rhee, E., Naumann, M., Dubiel, W., and Wolf, D.A. (2003). Fission yeast COP9/signalosome suppresses cullin activity through recruitment of the deubiquitylating enzyme Ubp12p. Mol. Cell *11*, 927–938.

Zorba, A., Nguyen, C., Xu, Y., Starr, J., Borzilleri, K., Smith, J., Zhu, H., Farley, K.A., Ding, W., Schiemer, J., et al. (2018). Delineating the role of cooperativity in the design of potent PROTACs for BTK. Proc. Natl. Acad. Sci. USA *115*, E7285–E7292.

STAR★METHODS

KEY RESOURCES TABLE

REAGENT or RESOURCE	SOURCE	IDENTIFIER
Antibodies		
COPS8	Santa Cruz Biotechnology	Cat# sc-393482
CAND1	Santa Cruz Biotechnology	Cat# sc-137055; RRID: AB_2068847
UBE2M	Santa Cruz Biotechnology	Cat# sc-390064
CUL4A	Cell Signaling Technology	Cat# 2699S; RRID: AB_2086563
CUL2	Sigma-Aldrich	Cat# SAB2501565-100; RRID: AB_10959330
CRBN	F. Bassermann lab; Eichner et al., 2016	N/A
VHL	Cell Signaling Technology	Cat# 2738; RRID: AB_2218190
B-ACTIN	Sigma-Aldrich	Cat# A5441; RRID: AB_476744
BRD4	Bethyl Laboratories	Cat# A301-985A100; RRID: AB_2620184
CDK9	Cell Signaling Technology	Cat# 2316S; RRID: AB_2291505
GSPT1	Abcam	Cat# ab49878; RRID: AB_2115507
RBM39	Santa Cruz Biotechnology	Cat# sc-376531; RRID: AB_11150838
HA	Cell Signaling Technology	Cat# 3724S; RRID: AB_1549585
Ubiquitin	Cell Signaling Technology	Cat# 3933S; RRID: AB_2180538
FLAG	Cell Signaling Technology	Cat# 2368S; RRID: AB_2217020
H3	Abcam	Cat# 1791; RRID: AB_302613
anti-mouse secondary antibody	Jackson ImmunoResearch	Cat# 115-035-003; RRID: AB_10015289
anti-rabbit secondary antibody	Jackson ImmunoResearch	Cat# 111-035-003; RRID: AB_2313567
anti-goat secondary antibody	Jackson ImmunoResearch	Cat# 705-035-147; RRID: AB_2313587
Chemicals, Peptides, and Recombinant Proteins		
Degrader of BET proteins: ARV-771	MedChemExpress; Raina et al., 2016	Cat# HY-100972
GSPT1 degrader: CC-885	AxonMedChem; Matyskiela et al., 2016	Cat# 2645
RBM39 degrader: indisulam	Sigma-Aldrich; Han et al., 2017; Uehara et al., 2017	Cat# SML1225
Degrader of BET proteins: dBET6	N.S. Gray lab; Winter et al., 2017	N/A
CDK9 degrader: THAL-SNS-032	N.S. Gray lab; Olson et al., 2018	N/A
NEDD8-Activating Enzyme (NAE) inhibitor: MLN4924	Selleckchem; Soucy et al., 2009	Cat# S7109
COPS5 inhibitor: CSN5i-03	Kindly provided by Novartis; Schlierf et al., 2016	N/A
Carfilzomib	Selleckchem	Cat# S2853
TAK-243	MedChemExpress	Cat# HY-100487
NEM	Sigma-Aldrich	Cat# E3876
dTAG-7	Synthesized in-house; Erb et al., 2017	N/A
biotin-phenol	Iris Biotech	Cat# LS-3500
sodium ascorbate	Sigma-Aldrich	Cat# A4034
sodium azide	Sigma-Aldrich	Cat# S2002
Trolox	Sigma-Aldrich	Cat# 238813
Critical Commercial Assays		
DNeasy Blood & Tissue mini kits	Quiagen	Cat# 69504
ExTaq polymerase	Clontech	Cat# RR001C

(*Continued on next page*)

Continued

REAGENT or RESOURCE	SOURCE	IDENTIFIER
AMPure XP beads	Beckman Coulter	Cat# A63880
Qubit dsDNA HS Assay Kit	Thermo Fisher	Cat# Q32854
CellTiter Glo	Promega	Cat# G7570
anti-FLAG M2 magnetic beads	Sigma-Aldrich	Cat# M8823-1ML
μ-Slide	Ibidi	Cat# 80826
Lipofectamine 2000	Invitrogen	Cat# 11668019
streptavidin magnetic beads	Thermo Fisher Scientific	Cat# 11205D
protease inhibitors	Thermo Fisher Scientific	Cat# 78437
DMEM	Lonza	Cat# 12-708F
IMDM	Lonza	Cat# 12-915F
RPMI	Thermo Fisher Scientific	Cat# 11875-085
polylysine	Sigma-Aldrich	Cat# P8920
PolyFect	Quiagen	Cat# 301105
Lenti-X-concentrator	Takara	Cat# 631232
Deposited Data		
Sequencing of sgRNA cassettes in genome-scale CRISPR/Cas9 screens	This paper	NCBI Sequence Read Archive (SRA): SRP169964
Experimental Models: Cell Lines		
KBM7	T. Brummelkamp lab; Carette et al., 2009	N/A
293T	ATCC	CRL-3216
MV4;11	ATCC	CRL-9591
AsPC1	ATCC	CRL-1682
RKO	ATCC	CRL-2577
Oligonucleotides		
sgRNAs for validation of 11 hits, see Table S1	This paper	N/A
sgCUL4A for validation of SR autodegradation, see Table S1	This paper	N/A
primers used to characterize single mutant clones, see Table S1	This paper	N/A
primers used to clone APEX2 into a Gateway compatible donor vector, see Table S1	This paper	N/A
Primers for next generation sequencing library preparation, see Table S4	This paper	N/A
Recombinant DNA		
Brunello pooled library	Addgene	#73178; 2-vector system
pMD2.G	Addgene	#12259
psPAX2	Addgene	#12260
Lenti_Cas9_Blasti	Addgene	#52962
lentiGuide-Puro	Addgene	#52963
LRG (Lenti_sgRNA_EFS_GFP)	Addgene	#65656
lentiGuide-Puro-IRES-mCherry	G. Superti-Furga Lab Modified from Addgene #52963	N/A
pHIV_dTOMATO	Addgene	#21374
pHIV_eGFP	Addgene	#21373
pLX305-mCherry-dTAG	This paper	
pcDNA3-FLAG-CRBN	Addgene	#107380
pcDNA3-HA-Ub	Addgene	#18712
pLX305-APEX2-dTAG	This paper	

(*Continued on next page*)

Continued

REAGENT or RESOURCE	SOURCE	IDENTIFIER
Software and Algorithms		
cutadapt	Martin, 2011	https://cutadapt.readthedocs.io/en/stable/
fastx_trimmer		http://hannonlab.cshl.edu/fastx_toolkit/
Bowtie2	Langmead and Salzberg, 2012	http://bowtie-bio.sourceforge.net/bowtie2/index.shtml
STARS v1.3 algorithm	Doench et al., 2016	https://portals.broadinstitute.org/gpp/public/software/stars
GOrilla	Eden et al., 2009	http://cbl-gorilla.cs.technion.ac.il/
GraphPad Prism		https://www.graphpad.com/
FlowJo		https://www.flowjo.com/

LEAD CONTACT AND MATERIALS AVAILABILITY

Further information and requests for resources and reagents should be directed to and will be fulfilled by the Lead Contact, Georg E. Winter (gwinter@cemm.oeaw.ac.at).

EXPERIMENTAL MODEL AND SUBJECT DETAILS

Cell lines

KBM7 cells (Carette et al., 2009) with the specified genetic backgrounds were grown in IMDM supplemented with 10% FBS and 1% penicillin/streptomycin (pen/strep). AsPC1, RKO and 293T cells were grown in DMEM 10% FBS and 1% pen/strep. MV4;11 cells were grown in RPMI 10% FBS, 1% pen/strep. KBM7, RKO and MV4;11 cells expressing Cas9 were generated using the plasmid Lenti_Cas9_Blasti (Addgene #52962). For screen validation purposes, the lentiviral plasmids lentiGuide-Puro (Addgene #52963) or LRG (Lenti_sgRNA_EFS_GFP) (Addgene #65656) were used to express sgRNAs (see Table S1 and corresponding methods section below) in KBM7-Cas9 cells. The lentiviral plasmid lentiGuide-Puro-IRES-mCherry (modified from Addgene #52963) was used to express sgRNAs against *CUL4A* (see Table S1 and corresponding methods section below).

METHOD DETAILS

Brunello lentivirus production

4 million 293T cells were seeded on 10cm culture plates 16h before plasmid transfection. Cells at ~80% confluence were transfected with 5μg Brunello pooled library (Addgene #73178; 2-vector system), 2.5μg pMD2.G (Addgene #12259), and 3.75μg psPAX2 (Addgene #12260) using PolyFect (QIAGEN) according to the manufacturer's protocol. Medium was replaced by fresh DMEM (10% FBS, 1% pen/strep) 8h after transfection. Viral supernatant was harvested 48 and 72h after transfection and 20x concentrated using Lenti-X-concentrator (Takara), according to the manufacturer's protocol. Concentrated viral supernatant was stored in aliquots at −80°C and titrated to achieve a MOI of 0.2-0.3.

Brunello pooled library screens

180 million KBM7-Cas9 cells were transduced at MOI 0.23, yielding a calculated library representation of 535 cells/sgRNA (library representation = 40 million cells). For transduction, 100μL of concentrated viral supernatant was added to 3 million cells in 3 mL IMDM and 8μg/mL polybrene in 12-well plates (total of 5 plates; viral supernatant was omitted in one well for titrating transduction efficiency). Plates were centrifuged at 2000rpm for 1h at 30°C in a benchtop centrifuge and then incubated at 37°C overnight. The next day, transduced cells were pooled and diluted to 750,000 cells/mL in five T150 flasks. Transduction efficiency was titrated following a standard protocol (Doench et al., 2016). Pools were selected with 1μg/mL puromycin for 15 days, splitting them every 5 days to maintain exponential growth.

Five independent resistance screens were performed with the library. The small-molecule degraders used were:

ARV-771 (MedChemExpress, HY-100972), CC-885 (AxonMedChem, 2645), indisulam (Sigma-Aldrich, SML1225), dBET6 and THAL-SNS-032 (kindly provided by Nathanael S. Gray, Dana Farber Cancer Institute). Selective drug treatment was performed on 40 million cells/drug at a seeding density of 500,000 cells/mL. Starting drug concentrations were previously titrated to yield an intermediate effect on cell growth by counting cells and re-treating every 4 days from 5000x drug stocks. Used starting concentrations for the resistance screens were: 15nM dBET6, 15nM ARV-771, 0.75nM CC-885, 50nM THAL-SNS-032, 300nM indisulam, and a respective DMSO control. Every 4 days, cells were pooled, counted and re-seeded to 40 million cells in 80mL, applying fresh drug. Drug concentrations were dynamically adjusted to the growth curves to yield a consistent impact on cell proliferation: dBET6 concentration was raised to 20nM after day 8; CC-885 was raised to 0.9nM after day 4; THAL-SNS-032 was raised to 60nM after day 8;

indisulam was lowered to 200nM after day 8; ARV-771 was raised to 20nM after day 8. Drug resistant pools were harvested after 20 days of treatment, purified using Lonza lymphocyte separation medium, and allowed to recover in drug-free IMDM (10% FBS, 1% pen/strep) overnight. The next day, cell pellets were collected by centrifugation, snap-frozen in liquid nitrogen and stored at −80°C.

Library preparation for next generation sequencing

Genomic DNA (gDNA) was extracted from 40 million cell frozen pellets using DNeasy Blood & Tissue mini kits (QIAGEN), according to the manufacturer's protocol. DNA concentration was quantified by NanoDrop and total yield was between 340 and 450μg. PCR on the genomic DNA templates was performed to amplify sgRNA sequences, following a published protocol (Doench et al., 2016). The total amount of isolated gDNA was processed in parallel to yield 10μg gDNA per 100μL reaction. One PCR reaction contained 1.5μL of ExTaq polymerase (Clontech), 10μL of provided 10x buffer, 8μL of provided dNTP mix, 0.5μL of 100μM P5 forward primer mix (staggered to improve sequencing run complexity), 10μL of 5μM condition-specific P7 barcoded primer, and water to reach 100μL. DNA oligo primers were ordered PAGE purified from Sigma Aldrich (Table S4). Target amplification was achieved by using the following program: 1 minute at 95°C initial denaturation; 30 s at 95°C, 30 s at 53°C, 30 s at 72°C, for 26-27 cycles; 10 minutes at 72°C final elongation. Specific amplification of the 360bp target was confirmed by agarose gel electrophoresis. All PCR reactions of a respective condition were pooled and 100μL were purified using AMPure XP beads in a 1:1 ratio, following standard protocols. Purified amplicon was eluted using 50μL TE buffer and DNA concentration was Qubit quantified to 16-36 ng/μL (Qubit dsDNA HS Assay Kit, Thermo Fisher Q32854). Final sequencing libraries were pooled in equimolar amounts, diluted to 5ng/μL and sequenced on a HiSeq 3000/4000 to yield ∼60-120 million raw reads.

Next generation sequencing data analysis

De-multiplexed raw reads were processed to count sgRNA spacer abundance using a custom script. Raw FASTQ reads were trimmed with cutadapt (Martin, 2011) using *-g CGAAACACCG–minimum-length = 10* to remove the sequence immediately 5′ of the spacer. The first 20bp of the trimmed reads were collected using fastx_trimmer *–l 20* (http://hannonlab.cshl.edu/fastx_toolkit/) and aligned against the Brunello spacer index using Bowtie2 (Langmead and Salzberg, 2012), allowing one mismatch with *–N1*. Spacers were counted using *cut –f 3 | sort | uniq –c* on the aligned SAM files. A count table with all drug conditions was then assembled and normalized to counts-per-million. Log2 fold changes of drug treatment versus DMSO were calculated from normalized counts, omitting spacers with no reads in the DMSO condition. The enrichment rank of each spacer sequence was expressed as a fraction of the total number of spacers, so that the most enriched spacer is assigned a perturbation strength of 1, in accordance with the STARS algorithm (Doench et al., 2016). Gene hits were called using the STARS v1.3 algorithm (Doench et al., 2016) with options *–dir P–thr 10–use-first-pert N*, testing against a null hypothesis of 5,000 permutations (Table S5). Manual curation of cross-library contaminating reads was performed for specific SRs that were detected in non-related screens. Hits with a q-value lower than 0.2 were deemed significant and used for further network-based analysis.

Interactome construction

Hits from the five independent screens were used to generate a network reporting gene-drug and protein-protein interactions. The protein-protein interaction (PPI) network was built from interactions reported in the Human Integrated Protein-Protein Interaction Reference (HIPPIE) database (Alanis-Lobato et al., 2017). Only protein coding genes with documented author and Pubmed reference were included. The resulting network consisted of N = 15847 proteins connected via M = 259196 edges. Mapping our hits on this network, we got a subnetwork consisting of N = 77 proteins connected via M = 76 edges.

In addition, we generated an expanded network: Given experimental limitations, essentiality, and imposed cutoffs, not all genes conferring resistance to drug exposure can be identified unambiguously. We used a network-driven approach to identify possible sub-threshold genes. This approach is an adaptation of an algorithm designed to detect network modules (Ghiassian et al., 2015). First, we defined a list of candidates from all the first neighbors of the hit list that are also essential (genes with at least two guides resulting in fold changes above the 95th percentile cutoffs were classified as essential). For each candidate, we calculated the significance of the number of connections to the hit list using a hypergeometric model. That is, for each candidate gene with overall degree k and k_s links to the s_0 hit list genes, we calculated the connectivity p value given by the cumulative probability.

$$p_{candidate} = \sum_{i=k_s}^{k} \frac{\binom{s_0}{i}\binom{N-s_0}{k-i}}{\binom{N}{k}}$$

Final p values for each gene were Bonferroni corrected. From the candidate list, we selected the genes with $p_{corrected} < 0.05$ (19 genes). The resulting network with the expanded hit lists consists of N = 96 proteins connected via M = 274 edges.

Gene Ontology enrichment analysis

GOrilla (Eden et al., 2009) was used to identify Gene Ontology (GO) terms enriched in the dataset of screen hits (q-value < 0.2) as compared to genome-wide representation. Ranking mode: Two unranked lists of genes (target and background lists), searching for GO terms that are enriched in the target set (screen hits) compared to the background set using the standard Hyper Geometric statistics. Ontology: Biological process and cellular component. P value threshold: 0.001.

Competition growth experiments

KBM7-Cas9 cells were transduced with vectors expressing either dTomato (pHIV_dTOMATO, Addgene #21374) or eGFP (pHIV_eGFP, Addgene #21373). The lentiviral plasmid lentiGuide-Puro (Addgene #52963) was used to express sgRNAs against selected hits (2 sgRNAs per gene, see Table S1). dTomato+ cells were transduced with control sgRNAs and eGFP+ cells with sgRNAs against 11 hits, and mixed at a ratio ~50:50. The mixed populations were grown in the presence of DMSO or the respective degrader for 14 days, and monitored by flow cytometry every 7 days. First, each hit was only tested against the degrader(s) found to confer resistance to (dBET6 20nM, CC-885 1nM, THAL-SNS-032 50nM, indisulam 250nM, ARV-771 20nM). Then, we prioritized selected genes (UBE2M, CAND1, COPS1, COPS7B, and COPS8) and repeated competition growth experiments against all screened degraders. RKO-Cas9 and MV4;11-Cas9 cells were transduced with lentiviruses expressing sgRNAs against UBE2M, CAND1 or COPS8 in the GFP vector LRG (Lenti_sgRNA_EFS_GFP) (Addgene #65656). GFP-expressing cells were mixed with GFP-negative cells at a ratio ~50:50. The mixed populations were grown in the presence of DMSO or degrader for 15 days, and monitored by flow cytometry at day 0 and 15. Degrader doses for MV4;11 cells were the same than for KBM7 cells. Degrader doses were dynamically adjusted for RKO cells up to reach doses of ~4x EC_{50}: dBET6 80nM, CC-885 400nM, THAL-SNS-032 360nM, ARV-771 40nM). Data was analyzed with the FlowJo software and represented with Prism (GraphPad software).

Isolation and characterization of single mutant clones

WT and mutant clones ($UBE2M^{mut}$, $CAND1^{mut}$, $COPS1^{mut}$, $COPS7B^{mut}$, $COPS8^{mut}$, $CRBN^{mut}$) were isolated via low density plating, expanded and pellets were collected for further characterization. gDNA was extracted and PCR was conducted to amplify sequence products of ~700bp covering the expected Cas9 cutting site. The primers used are described in Table S1. Editing outcomes were monitored by Sanger sequencing (Microsynth).

Cell viability assays

WT and mutant KBM7 clones ($UBE2M^{mut}$, $CAND1^{mut}$, $COPS1^{mut}$, $COPS7B^{mut}$, $COPS8^{mut}$ and $CRBN^{mut}$) were seeded at a cell density of 50,000 cells/mL in 96-well plates and treated with DMSO or 9 concentrations of each degrader, NVP2 or JQ1, in triplicate (1:4 dilutions starting from 10μM, with the exception of CC-885 1μM and indisulam 50μM). Cells were treated for 3 days, after which a cell viability assay was performed (CellTiter Glo, Promega), according to manufacturer's protocol. Survival curves were calculated by best-fit analysis of the log10 drug concentration to fold change of drug-treated cells over DMSO-treated cells. All survival assays included technical triplicates per sample, per experiment. Data were represented with Prism (GraphPad software).

Western blot analysis

Cell pellets were lysed in 50mM Tris pH 7.9, 8M Urea and 1% CHAPS and incubated with shaking at 4°C for at least 30min. 20 μg of supernatants were run and transferred for detection by using the corresponding antibodies. Antibodies used: COPS8 (1:500, Santa Cruz Biotechnology sc-393482), CAND1 (1:500, Santa Cruz Biotechnology sc-137055), UBE2M (1:500, Santa Cruz Biotechnology sc-390064), CUL4A (1:1,000, Cell Signaling Technology 2699S), CRBN (1:2000, kind gift of R. Eichner and F. Bassermann) (Eichner et al., 2016), VHL (1:500, Cell Signaling Technology 2738), CUL2 (1:500, Sigma-Aldrich SAB2501565-100), ACTIN (1:10,000, Sigma-Aldrich A5441), BRD4 (1:5,000, Bethyl Laboratories A301-985A100), CDK9 (1:500, Cell Signaling Technology 2316S), GSPT1 (1:1,000, Abcam ab49878), RBM39 (1:500, Santa Cruz Biotechnology sc-376531), HA (1:2,000, Cell Signaling Technology 3724S and 2367S), Ubiquitin (1:1,000, Cell Signaling Technology 3933S), FLAG (1:1,000 Cell Signaling Technology 2368S) and H3 (1:10,000 Abcam 1791). Secondary antibodies (1:5,000, anti-mouse Jackson ImmunoResearch 115-035-003 and anti-rabbit Jackson ImmunoResearch 111-035-003).

Drug treatments for target degradation assessment

2 million KBM7 cells (WT or mutant genetic backgrounds) were used per condition, resuspended in 2mL of IMDM and incubated in 12-well plates, with DMSO or chemical degrader (dBET6, CC-885, THAL-SNS-032, indisulam or ARV-771) and with/without the NEDD8-Activating Enzyme (NAE) inhibitor MLN4924 (Soucy et al., 2009) (Selleckchem, S7109) or with the COPS5 inhibitor CSN5i-03 (Schlierf et al., 2016). Times and doses of the treatments are specified in the corresponding figure legends. After the treatments, cells were collected and processed for western blot (WB) analysis.

mCherry-dTAG reporter: live cell imaging and flow cytometry

The lentiviral reporter vector pLEX305-mCherry-dTAG was generated by Gateway cloning (Invitrogen) using the compatible vectors pDONR221_mCherry_C and pLEX_305-N-dTAG (Addgene #91797). To evaluate mCherry-dTAG degradation by time-lapse microscopy, exponentially growing KBM7 WT, $COPS8^{mut}$, $CAND1^{mut}$ and $UBE2M^{mut}$ cells were transduced with lentiviruses expressing

pLEX305-mCherry-dTAG. The reporter cells were seeded on 8 wells μ-Slide (Ibidi, 80826) pre-treated with polylysine and centrifuged for 10min at 662 × g to attach. DMSO or 1μM dTAG-ligand (dTAG-7, synthetized in-house) was added to the corresponding wells and imaging was performed right after every minute for a total of 45 min in an Olympus IX83 system, software CellSens Dimension.

To quantify the degradation dynamics in a more high-throughput manner, we used flow cytometry. In brief, 30,000 cells per well were seeded in 96-well plates in a total volume of 100μL, and mCherry loss was evaluated after addition of DMSO or dTAG-ligand in a dose-resolved (2h with 32.3nM, 62.5nM, 125nM, 0.25μM, 0.5μM, 1μM, 2μM) and time-resolved manner (1μM for 10min, 20min, 30min, 1h, 2h, 4h), using a Fortessa flow cytometer analyzer. We repeated the flow cytometry experiments in KBM7 WT cells expressing mCherry-dTAG combining the dTAG-ligand with MLN4924 (Soucy et al., 2009) (1μM) or CSN5i-03 (Schlierf et al., 2016) (1μM).

Substrate receptor auto-degradation

2 million KBM7 cells per condition (WT or mutant genetic backgrounds, DMSO-, MLN4924- or CSN5i-03-treated cells) were collected and processed for WB analysis. Levels of the substrate receptors CRBN and VHL, and the neddylation status of CUL4A and CUL2 were evaluated by WB. Time and dose treatments with MLN4924 and CSN5i-03 are specified in the figure legends. The lentiviral plasmid lentiGuide-Puro-IRES-mCherry (modified from Addgene #52963) was used to express sg*CUL4A* (see Table S1) in KBM7 WT, UBE2M^{mut}, CAND1^{mut}, and COPS8^{mut} cells. The auto-degradation rescue was also evaluated in cells expressing sgRNAs against the CRL4^{CRBN}-bound E2 ligase UBE2G1 (pools) (lentiGuide-Puro Addgene #52963, see Table S1).

CRBN ubiquitination

2 million KBM7 WT cells per condition were pretreated for 30min with DMSO, MLN4924 1μM, Carfilzomib 1μM (Selleckchem S2853) or TAK-243 10μM (MedChemExpress HY-100487), then treated with either DMSO or CSN5i-03 100nM for 2h, collected and processed for WB analysis.

Immunoprecipitation

For FLAG-CRBN immunoprecipitation studies, two 10cm culture plates of 293T CRBN$^{-/-}$ cells (70%–80% confluent) were transfected with 2μg of pcDNA3-FLAG-CRBN (Addgene #107380) and 2μg of pcDNA3-HA-Ub (Addgene #18712) using Lipofectamine 2000 (Invitrogen 11668019). On the next day, cells were expanded to 4 10cm plates. 48h after transfection, cells were treated with either DMSO, Carfilzomib 1μM, CSN5i-03 2μM or Carfilzomib 1μM + CSN5i-03 2μM for 1h. Cells were collected and lysed in 200μl lysis buffer: 50mM Tris pH 7.5, 150mM NaCl, 0.1% NP40, 1mM EDTA, 5mM MgCl2, 5% Glycerol with protease inhibitors (Thermo Fisher Scientific, 78437) and NEM 20mM (Sigma-Aldrich E3876). After centrifugation at full speed for 20min, 250μg of protein per condition was incubated with 20μL of anti-FLAG M2 magnetic beads (Sigma-Aldrich M8823-1ML) for 1h at room temperature (beads were previously washed 3x in lysis buffer). After washing 2x with lysis buffer, elution was performed by boiling each sample in 60uL of 4x loading buffer supplemented with 10% β-mercaptoethanol for 7min. Beads were pelleted on a magnetic rack and eluate was collected, diluted 1:2 in lysis buffer and analyzed by WB.

Lists of putative substrate receptors associated to each cullin

In order to study the destabilization of cullin-specific SRs, we prepared lists with the putative SRs than can be incorporated into functionally competent CRLs segregated in cullin-related groups (see Table S2). For these nominations, we included all the members of the F-box family (according to the HGNC) (Braschi et al., 2019) as presumed SRs associating with CRL1 (Jin et al., 2004), VHL-box proteins as SRs binding to CRL2 (Kamura et al., 2004; Mahrour et al., 2008), BTB proteins (CRL3) (Chevrier and Corcoran, 2014; Dubiel et al., 2018; Pintard et al., 2004; Stogios et al., 2005), DCAF proteins (CRL4A/B) (He et al., 2006; Lee and Zhou, 2007), SOCS-box proteins (CRL5) (Kamura et al., 2004) and the F-box protein FBXO7 as SR engaging with CRL7 (Dias et al., 2002). In total, we considered 317 different proteins as potential SRs. In our proteomics experiments 159 of those putative SRs were detected and therefore used in subsequent analysis.

Expression proteomics

First, we compared overall proteome-wide changes in COPS8^{mut}, CAND1^{mut} and KBM7WT cells, using quantitative proteomics based on isobaric tagging. Second, we compared KBM7 WT cells treated with DMSO or CSN5i-03 (1μM, 8h). Third, we profiled MV4;11 and AsPC1 cells treated with DMSO or CSN5i-03 (1μM, 8h).

Sample preparation

50x10^6 KBM7, 30x10^6 MV4;11 or 30x10^6 AsPC1 cells per condition were collected, washed four times with ice-cold DPBS, the supernatant aspirated and pellets snap-frozen in liquid N2. Each washed cell pellet was lysed separately in 40 μL of freshly prepared lysis buffer containing 50 mM HEPES (pH 8.0), 2% SDS, 0.1 M DTT, 1 mM PMSF, and protease inhibitor cocktail (Sigma-Aldrich). Samples rested at RT for 20 minutes before heating to 99°C for 5 min. After cooling down to RT, DNA was sheared by sonication using a Covaris S2 high performance ultrasonicator. Cell debris was removed by centrifugation at 20.000 × g for 15 min at 20°C. Supernatent was transferred to fresh eppendorf tubes and protein concentration determined using the BCA protein assay kit (Pierce Biotechnology, Rockford, IL). FASP was performed using a 30 kDa molecular weight cutoff filter (VIVACON 500; Sartorius Stedim Biotech GmbH, 37070 Goettingen, Germany) essentially according to published procedures (Wiśniewski et al., 2009). In brief,

100 μg total protein per sample were reduced by adding DTT at a final concentration of 83.3 mM followed by incubation at 99°C for 5 min. After cooling to room temperature, samples were mixed with 200 μL of freshly prepared 8 M urea in 100 mM Tris-HCl (pH 8.5) (UA-solution) in the filter unit and centrifuged at 14.000 × g for 15 min at 20°C to remove SDS. Any residual SDS was washed out by a second washing step with 200 μL of UA. The proteins were alkylated with 100 μL of 50 mM iodoacetamide in the dark for 30 min at RT. Afterward, three washing steps with 100 μL of UA solution were performed, followed by three washing steps with 100μL of 50 mM TEAB buffer (Sigma-Aldrich). Proteins were digested with trypsin at a ratio of 1:50 overnight at 37°C. Peptides were recovered using 40 μL of 50 mM TEAB buffer followed by 50 μL of 0.5 M NaCl (Sigma-Aldrich). Peptides were desalted using C18 solid phase extraction spin columns (The Nest Group, Southborough, MA). After desalting, peptides were labeled with TMT 10plex reagents according to the manufacturer (Pierce, Rockford, IL). After quenching of the labeling reaction, labeled peptides were pooled, organic solvent removed in vacuum concentrator and labeled peptides cleaned via C18 solid phase extraction (SPE).

Offline Fractionation via RP-HPLC at high pH

Tryptic peptides were re-buffered in 20 mM ammonium formiate buffer pH 10, shortly before separation by reversed phase liquid chromatography at pH 10 as described (Gilar et al., 2005). Peptides were separated into 96 time-based fractions on a Phenomenex C18 RP column (150 × 2.0 mm Gemini-NX 3 μm C18 110Å, Phenomenex, Torrance, CA, USA) using an Agilent 1200 series HPLC system fitted with a binary pump delivering solvent at 100 μL/min. Acidified fractions were consolidated into 36 fractions via a concatenated strategy described (Wang et al., 2011). After solvent removal in a vacuum concentrator, samples were reconstituted in 5% formic acid for LC-MS/MS analysis and kept at −80°C until analysis.

2D-RP/RP Liquid Chromatography Mass Spectrometry

Mass spectrometry was performed on an Orbitrap Fusion Lumos mass spectrometer (ThermoFisher Scientific, San Jose, CA) coupled to a Dionex Ultimate 3000RSLC nano system (ThermoFisher Scientific, San Jose, CA) via nanoflex source interface. Tryptic peptides were loaded onto a trap column (Pepmap 100 5 μm, 5 × 0.3 mm, ThermoFisher Scientific, San Jose, CA) at a flow rate of 10 μL/min using 2% ACN and 0.05% TFA as loading buffer. After loading, the trap column was switched in-line with a 40 cm, 75 μm inner diameter analytical column (packed in-house with ReproSil-Pur 120 C18-AQ, 3 μm, Dr. Maisch, Ammerbuch-Entringen, Germany). Mobile-phase A consisted of 0.4% formic acid in water and mobile-phase B of 0.4% formic acid in a mix of 90% acetonitrile and 9.6% water. The flow rate was set to 230 nL/min and a three-step 90 min gradient applied (6 to 30% solvent B within 81 min, 30 to 65% solvent B within 8 min and, 65 to 100% solvent B within 1 min, 100% solvent B for 6 min before equilibrating at 6% solvent B for 18 min prior to next injection). Analysis on the MS was performed in a data-dependent acquisition (DDA) mode using a max 3 s cycle time. Full MS^1 scans were acquired in the Orbitrap with a scan range of 375 - 1650 m/z and a resolution of 120,000 (at 200 m/z). Automatic gain control (AGC) was set to a target of 2×10^5 and a maximum injection time of 50 ms. MS^2 -spectra were acquired in the Orbitrap at a resolution of 50,000 (at 200 m/z) with a fixed first mass of 100 m/z. In order to achieve maximum proteome coverage, a classical tandem MS approach was chosen (TMT reporter ion intensities extracted from MS^2-scans) instead of the available synchroneous precursor selection (SPS)-MS3 approach. The latter provides on average better TMT ratio accuracies but suffers from prolonged duty cycles and reduced identification rates. To minimize TMT ratio compression effects by interence of contaminating coeluting isobaric peptide ion species, precursor isolation width in the quadrupole was set to 0.4 Da and an extended fractionation scheme applied (36 fractions, see above). Monoisotopic peak determination was set to peptides with inclusion of charge states between 2 and 7. Intensity threshold for MS^2 selection was set to 5×10^4. Higher energy collision induced dissociation (HCD) was applied with a normalized collision energy (NCE) of 38%. AGC was set to 1×10^5 with a maximum injection time of 105 ms. Dynamic exclusion for selected ions was 60 s. A single lock mass at m/z 445.120024 was employed. Xcalibur version 4.2.28.14 and Tune 3.1 2412.17 were used to operate the instrument.

Data Analysis

Acquired raw data files were processed using the Proteome Discoverer 2.2.0 platform, utilizing the Sequest HT database search engine and Percolator validation software node (V3.04) to remove false positives with a false discovery rate (FDR) of 1% on peptide and protein level under strict conditions. Searches were performed with full tryptic digestion against the human SwissProt database v2017.06 with up to two allowed miscleavage sites. Oxidation (+15.9949Da) of methionine was set as variable modification, while carbamidomethylation (+57.0214Da) of cysteine residues and TMT labeling of peptide N-termini and lysine residues were set as fixed modifications. Data was searched with mass tolerances of ± 10 ppm and ± 0.02Da on the precursor and fragment ions, respectively. Results were filtered to include peptide spectrum matches (PSMs) with Sequest HT cross-correlation factor (Xcorr) scores of ≥ 1 and high peptide confidence assigned by Percolator. MS^2 signal-to-noise values (S/N) values of TMT reporter ions were used to estimate peptide/protein abundance changes. PSMs with precursor isolation interference values of $\geq 50\%$ and average TMT-reporter ion S/N ≤ 10 were excluded from quantitation. Only unique peptides were used for TMT quantitation as well as for TOP3 label-free quantitation. Isotopic impurity correction and TMT channel-normalization based on total peptide amount were applied. For statistical analysis and p value calculation, the integrated ANOVA hypothesis test was used. TMT ratios with p values below 0.01 were considered as significant. Only proteins with > 1 peptide detected and > 1 unique peptide detected were considered for further analysis.

For the calling of destabilized substrate receptors, a log2 fold change threshold (CSN5i/DMSO) of −0.3 was applied. The comparison of destabilized substrate receptors in KBM7, AsPC1 and MV4;11 cells was performed on proteins detected across all cell lines (Table S3). Absolute protein abundance estimates were derived from protein specific TOP3 scores (Silva et al., 2006) calculated for the sum of all TMT channels. Each protein specific TOP3 score was subsequently multiplied with each sample specific TMT ratio to obtain estimates of protein abundance for each sample.

Drug treatments for ligand-mediated CRBN re-stabilization and protection from CRBN auto-degradation

For ligand-mediated CRBN re-stabilization experiments, 2 million KBM7 WT cells were used per condition, resuspended in 2mL of IMDM in 12-well plates and pre-treated for 2h with DMSO or CSN5i-03 (25nM and 100nM). After 2h of CSN5i-03 treatment CRBN was destabilized, and cells were treated for 0h, 1h or 2h with the chemical degraders CC-885 (500nM), THAL-SNS-032 (500nM) or dBET6 (250nM), to induce CRBN re-stabilization. After the treatments, cells were collected and processed for WB analysis.

For experiments assessing ligand-mediated protection from CRBN auto-degradation, 2 million KBM7 WT cells were used per condition, resuspended in 2mL of IMDM in 12-well plates and pre-treated for 15min or 30min with CC-885 (250nM), after which the cells were treated with CSN5i-03 (100nM, 2h). After the treatments, cells were collected and processed for WB analysis.

APEX2-dTAG experiments

The lentiviral vector pLEX305-APEX2-dTAG was generated through regular Gateway cloning (Invitrogen). First, APEX2 was cloned into a Gateway compatible donor vector (pDONR221) using BP clonase after PCR with primers containing BP overhangs (see Table S1 for primer sequences; APEX2 was PCR amplified from pcDNA3-APEX2-NES - Addgene #49386), to finally assemble the pENTR221_FLAG_APEX2_nonSTOP vector. Then, we performed a Gateway LR reaction with pENTR221_FLAG_APEX2_nonSTOP and pLEX305-N-dTAG (Addgene #91797), according to manufacturer's protocol. KBM7 cells were transduced with pLEX305-APEX2-dTAG lentiviruses to generate KBM7$^{APEX2\text{-}dTAG}$ cells.

The protocol used was initially based in a previously described protocol (Hung et al., 2016) and optimized for APEX2-dTAG experiments in KBM7 cells. An entire 6-welll plate pre-coated with polylysine was used per condition. Per well, 10 million KBM7$^{APEX2\text{-}dTAG}$ cells were resuspended in 1.5mL of IMDM in the presence of 250μM biotin-phenol (Iris Biotech, LS-3500) and centrifuged for 10min at 662 × g to attach KBM7 cells and facilitate washing steps before collecting pellets. Cells were shortly incubated at 37°C with DMSO or CSN5i-03 (1μM, 20min) with the purpose of inducing hyper-neddylation of CUL4A/B without time enough to induce CRBN auto-degradation. The last 5min of the incubation, DMSO or dTAG-ligand (1μM, 5min) was added to the cells, to induce ternary complex formation but without time enough to induce the degradation of APEX2-dTAG. Then, *in situ* proximity labeling was performed upon addition of freshly prepared H_2O_2 in DPBS (final concentration 1mM) for 1min at RT. Labeling solution was quickly aspirated and 5 washing steps on ice with freshly prepared quenching buffer were performed before scrapping and collecting the cells. Quenching buffer: 10mM sodium ascorbate (Sigma-Aldrich, A4034), 10mM sodium azide (Sigma-Aldrich, S2002), and 5M Trolox (Sigma-Aldrich, 238813) in DPBS. After centrifugation and aspiration of the supernatant, pellets were snap-frozen in liquid N2. Each pellet was lysed in 250 μL of RIPA supplemented with protease inhibitor, benzonase and quenchers (10mM sodium ascorbate, 10mM sodium azide and 5M Trolox). After resuspension, samples were left on ice for 15min and lysates clarified by centrifuging at 15,000 g for 10min at 4°C. Protein was quantified using the Bradford assay (BioRad). For streptavidin pull-down of the biotinylated proteins, 250μg of protein per sample was incubated with 60μL of streptavidin magnetic beads (Thermo Fisher Scientific, 11205D) for 1h at RT on a rotator. We added additional 500 μL of RIPA buffer to facilitate rotation. Beads were pelleted using a magnetic rack and each bead sample was washed twice with RIPA, once with 1M KCl, once with 0.1M Na_2CO_3, once with 2M urea in 10mM Tris-HCl pH 8, and twice with RIPA (wash buffers were maintain on ice). Biotinylated proteins were eluted from the beads by boiling each sample in 30uL of 3x loading buffer supplemented with 10% β-mercaptoethanol for 15min. Beads were pelleted on a magnetic rack and eluate was collected, diluted 1:2 in RIPA and analyzed by WB.

QUANTIFICATION AND STATISTICAL ANALYSIS

Statistical tests are specified in the corresponding figure legends and method sections, and error bars, cutoffs, number of replicates or samples, and number of independent experiments are detailed. Error bars are shown for all data points with replicates to represent the variation of each group.

DATA AND CODE AVAILABILITY

Sequencing of sgRNA cassettes in the 5 genome-scale CRISPR/Cas9 screens (associated with Figures 1A, 1B, S1B, and S1C) have been deposited in the NCBI Sequence Read Archive (SRA) with the final accession code: SRP169964. The analyzed data are provided in Table S5.